Chromatin remodeler *Arid1a* regulates subplate neuron identity and wiring of cortical connectivity

Daniel Z. Doyle[1,2,3], Mandy M. Lam[1,2], Adel Qalieh[1,2], Yaman Qalieh[1,2], Alice Sorel[1,2], Owen H. Funk[1,2], Kenneth Y. Kwan[1,2,3]

1. Michigan Neuroscience Institute (MNI), University of Michigan, Ann Arbor, MI 48109, USA
2. Department of Human Genetics, University of Michigan, Ann Arbor, MI 48109, USA
3. Neuroscience Graduate Program, University of Michigan, Ann Arbor, MI 48109, USA

*Correspondence should be addressed to K.Y.K. (kykwan@umich.edu)

Abstract

Subplate neurons indispensably orchestrate the developmental assembly of cortical neural circuits. Here, by cell type-specific dissection of *Arid1a* function, we uncover an unexpectedly selective role for this ubiquitous chromatin remodeler in subplate neuron molecular identity and circuit wiring function. We find that pan-cortical deletion of *Arid1a*, but not sparse deletion, leads to mistargeting of callosal and thalamocortical connectivities reminiscent of subplate ablation. These miswiring phenotypes are concomitant with disrupted subplate neuron organization, morphogenesis, axons, and extracellular matrix. Mechanistically, *Arid1a* is required to establish the transcriptional identity of subplate neurons. Remarkably, cortical plate deletion of *Arid1a*, which spares subplate neurons, restores subplate axons and extracellular matrix, and is sufficient to extensively correct callosal and thalamocortical axon misrouting, revealing an axon guidance function of *Arid1a* centered on the subplate. Thus, *Arid1a* regulates the molecular identity and function of subplate neurons, and thereby non-cell autonomously mediates the formation of cortical connectivity during development.

Introduction

The subplate is a transient layer of the fetal cerebral cortex essential to the developmental wiring of cortical circuits (Allendoerfer and Shatz, 1994; Hoerder-Suabedissen and Molnar, 2015; Kostovic and Rakic, 1990; McConnell et al., 1989, 1994; Molnár et al., 1998; Molnár et al., 2020; Wang et al., 2010). During neurogenesis, cortical neural progenitor cells (NPCs) generate excitatory neurons following an orderly temporal progression, successively giving rise to subplate neurons, then deep layer neurons, then upper layer neurons (Kwan et al., 2012; Rakic, 1974). As the first neurons generated from embryonic cortex, subplate neurons establish emerging cortical axon tracts and form the earliest synapses (Allendoerfer and Shatz, 1994; Friauf et al., 1990; Kanold and Luhmann, 2010; Kostovic and Rakic, 1990; McConnell et al., 1989, 1994; Wess et al., 2017). Importantly, subplate neurons, which are positioned at the interface between newly post-migratory neurons and the developing white matter, serve key non-cell autonomous wiring functions in the formation of cortical circuits. Experimental subplate ablation during fetal development leads to misrouting of thalamocortical axons (Ghosh et al., 1990; Ghosh and Shatz, 1992, 1993) and disrupts formation of sensory maps (Kanold and Shatz, 2006). Perturbed subplate function has been hypothesized to contribute to cortical circuitry defects in disorders of brain development (Hoerder-Suabedissen et al., 2013; Serati et al., 2019). Mechanistically, subplate neurons non-cell autonomously mediate circuit wiring at least in part by extending the earliest cortical descending axons, which interact with ascending axons during pathfinding (as posited by the “handshake hypothesis”) (Blakemore and Molnar, 1990; Molnar and Blakemore, 1995) and contribute to their crossing of the pallial-subpallial boundary (Chen et al., 2012; Magnani et al., 2013; Shinmyo et al., 2015). Subplate neurons also secrete extracellular matrix components

required for axon guidance (Blakemore and Molnar, 1990; De Carlos and O'Leary, 1992; Kostovic and Rakic, 1990; McConnell et al., 1989; Sheppard et al., 1991). In addition, subplate neurons are required for early oscillatory activity, which may contribute to the maturation of cortical circuits (Kanold and Luhmann, 2010; Molnár et al., 2020). In postnatal ages, some subplate neurons undergo programmed cell death (Price et al., 1997), thereby serving a transient role in cortical development.

Despite the central position of subplate neurons in orchestrating cortical connectivities, the molecular determinants of subplate wiring function remain largely elusive. Previous studies have focused on genes selectively expressed in subplate neurons (Hoerder-Suabedissen et al., 2013; Oeschger et al., 2012), which are found to mediate subplate neuron specification, migration, and axon development (Arai et al., 2019; Caviness, 1982; Han et al., 2011; Hevner et al., 2001; Kwan et al., 2008; Lai et al., 2008; Rakic et al., 2006; Ratie et al., 2019; Tiong et al., 2019). Here, by cell type-specific dissection of cortical *Arid1a* function, we uncover a surprisingly selective role for a ubiquitously-expressed chromatin remodeler in establishing the molecular identity and mediating the non-cell autonomous circuit wiring function of subplate neurons.

Arid1a (*Baf250a*) encodes a key subunit of the Brg/Brahma-associated factors (BAF, or mammalian SWI/SNF) ATP-dependent chromatin remodeling complex. The BAF complex functions by mobilizing and repositioning nucleosomes along DNA, thereby mediating important processes such as transcriptional regulation and DNA repair (Hodges et al., 2016). Similar to some other chromatin remodeling complexes, the BAF complex is broadly, and likely ubiquitously, present in cells and organs (Olave et al., 2002). Widely-expressed chromatin remodelers, however, can function context- or cell type-dependently, for example via interactions with transcription factors (Ho and Crabtree, 2010). For BAF, cell type-dependent subunit compositions of the complex have been shown to play diverse roles in embryonic stem cells, NPCs, and post-mitotic neurons (Sokpor et al., 2017; Son and Crabtree, 2014). *Arid1a*, however, has not been found to be incorporated into the BAF complex in a cell type-specific way and its potential context-dependent roles remain to be fully explored.

Here, we leverage a conditional allele of *Arid1a* to cell type-specifically manipulate BAF complex function. We find that cortical deletion of *Arid1a* leads to widespread misrouting of callosal and thalamocortical axons phenotypically reminiscent of subplate ablation. In contrast to broad *Arid1a* deletion, sparse *Arid1a* deletion does not cell autonomously alter axon pathfinding, suggesting a non-cell autonomous function of *Arid1a* in axon guidance. Mechanistically, deletion of *Arid1a* disrupted the transcription of subplate neuron-enriched genes. *Arid1a* is thus selectively required to establish the molecular identity of subplate neurons. Remarkably, *Arid1a* deletion from NPCs after subplate neurogenesis, which preserves ARID1A in subplate neurons but leads to ARID1A loss from cortical plate neurons, restores subplate organization, axon projections, and extracellular matrix, and is sufficient to extensively rescue callosal and thalamocortical miswiring. Thus, the role of *Arid1a* in cortical circuit wiring is centered on the subplate. Together, our results support that *Arid1a* selectively regulates the molecular identity of subplate neurons, and thereby non-cell autonomously mediates the wiring of cortical axon tracts during circuit development.

Results

Mistargeting of intracortical, but not corticofugal, axons following *Arid1a* deletion from NPCs

Arid1a is broadly expressed in human and mouse tissues (Consortium, 2012; Consortium, 2015), starting at the 4-cell stage during embryonic development and persisting through adulthood (Flores-Alcantar et al., 2011; Gao et al., 2008; Yue et al., 2014). Published bulk and single-cell RNA-seq data support widespread expression of *ARID1A* during fetal cortical development (Kang et al., 2011; Nowakowski et al.,

2017). We analyzed ARID1A protein in the developing mouse cortex by immunostaining, which revealed broad ARID1A expression in ventricular zone (VZ) and subventricular zone (SVZ) NPCs, cortical plate (CP) post-mitotic neurons, and non-neuronal cell types from embryonic day (E)12.5 to postnatal day (P)0 (**Fig. 1A**). The expression of ARID1A in SOX2+ NPCs and RBFOX3+ (NEUN+) neurons (**Fig. S1A**), and the complete colocalization of ARID1A with DAPI DNA staining (**Fig. S1B**) at E14.5 is consistent with ubiquitous ARID1A expression in cortical cell types during development. Constitutive deletion of *Arid1a* leads to lethality on E6.5 in mice, likely as a result of failed mesoderm formation (Gao et al., 2008). We therefore leveraged a conditional *Arid1a* allele to investigate *Arid1a* function during brain development (Gao et al., 2008).

To conditionally delete *Arid1a* from the developing cortex, we used $Emx1^{Cre}$, which expresses Cre recombinase in cortical NPCs starting at ~E10.5, near the onset of cortical neurogenesis (**Fig. 1B**) (Gorski et al., 2002). Deletion of *Arid1a* was validated in $Emx1^{Cre/+}$;$Arid1a^{fl/fl}$ conditional mutants (**cKO-E**) by ARID1A immunostaining, which revealed loss of ARID1A from cortical NPCs and neurons of the *Emx1* lineage (**Fig. 1C**). ARID1A staining was preserved in ventral telencephalon. Mutant cKO-E mice were born at Mendelian ratio, had typical lifespan, and were fertile as adults. At P0, the size of cKO-E cortex was not significantly different from control littermates (**Fig. S1C**).

To assess the development of neocortical layers, we analyzed laminar markers by immunostaining of P0 brain sections (**Fig. 1D**). We found largely normal cortical lamination in *Arid1a* cKO-E; TBR1+ layer (L)6, BCL11B+ (CTIP2+) L5, and LHX2+ L2-5 neurons were properly ordered in cKO-E and not significantly different from P0 littermate control (ctrl) based on marker quantification (**Fig. S1D**) and analysis of cumulative distribution of layer markers through the thickness of the cortex (**Fig. 1D**). We noted, however, that a stereotyped gap in marker and DAPI staining was present in the upper cortical layers (L2-4) of all analyzed cKO-E brains (arrowheads, **Fig. 1D**, 3/3 animals) but absent from controls (0/3 animals). Interestingly, this gap was characterized by aberrant L1CAM-immunostained axons, suggesting the presence of misrouted axons in cKO-E cortex.

We next examined potential changes in axonal projections more broadly. To visualize cells that have undergone Cre recombination, we used the Cre-dependent fluorescent reporter allele $ROSA^{mTmG}$ (Muzumdar et al., 2007). Following $Emx1^{Cre}$ recombination, membrane-associated EGFP (mEGFP) was expressed from $ROSA^{mTmG}$ in all cortical excitatory neurons, enabling genetic anterograde tracing of their axon tracts (schematized in **Fig. 1E**). In P0 littermate ctrl cortex, mEGFP expression revealed the trajectory of the corpus callosum (CC), which homotopically connected the left and right cortical hemispheres, and the anterior commissure (AC), which connected lateral cortical regions (**Fig. 1F**). In striking contrast to ctrl, the corpus callosum did not form in cKO-E cortex, which was instead characterized by widespread misrouting of cortical axons, including radially-directed axons towards the pia (arrows, **Fig. 1F**) and tangentially-directed axons through the upper layers (arrowheads, **Fig. 1F**). These axon misrouting phenotypes were confirmed by immunostaining for L1CAM (**Fig. S1E**). In addition to the callosum, anterior commissure axons were also mistargeted in cKO-E, being aberrantly routed to ventral forebrain and unable to cross the midline (**Fig. 1F** and **S1F**). Quantitative analysis of callosal and commissural thickness revealed complete loss of these axon tracts at the midline in cKO-E (**Fig. 1G**).

We next used the $ROSA^{mTmG}$ anterograde tracing strategy to analyze corticofugal axons. In striking contrast to intracortical axons, corticofugal tracts (i.e. corticothalamic, corticotectal, and corticospinal) did not show apparent misrouting deficits in cKO-E (**Fig. 1H**). These tracts followed their normal trajectories out of the cortex, through the internal capsule (IC), and innervated their respective targets in dorsal thalamus, tectum, and medulla. Together, our genetic anterograde tracing analysis data revealed widespread mistargeting of intracortcal axon tracts, but not corticofugal axon tracts, following *Arid1a* deletion from cortical NPCs, implicating a tract-dependent role for *Arid1a* in cortical circuit development.

Non-cell autonomous misrouting of thalamocortical axons following *Arid1a* deletion

Cortical deletion of *Arid1a* tract-dependently disrupted cortical axons. To determine whether corticopetal axon tracts were altered in *Arid1a* cKO-E, we analyzed thalamocortical axons. Thalamocortical axons originate from thalamic neurons and target the cortex (schematized in **Fig. 2A**). In *Arid1a* cKO-E, the thalamocortical neurons were unaffected by *Emx1^{Cre}*; however, the target of these axons, the cortex, was broadly affected by *Emx1^{Cre}* deletion of *Arid1a*. To assess thalamocortical axon development, we first used cytochrome oxidase (CO) histochemistry on flattened P7 cortex to visualize the whisker barrels, a major target of somatosensory inputs carried by thalamocortical axons (TCA). In P7 ctrl, CO staining revealed discrete, stereotyped, and highly organized whisker barrels in primary somatosensory cortex (**Fig. 2B**). In contrast, the formation of barrels in cKO-E somatosensory cortex was severely disrupted; many barrels were missing and the remaining barrels were distorted and disorganized, suggesting a deficit in thalamocortical axon targeting. These cKO-E defects in barrel organization were confirmed by immunostaining for NTNG1 (Netrin G1), a marker of thalamocortical axons, on P7 coronal brain sections (**Fig. 2B**). In addition, analysis of P0 cKO-E cortex further revealed that NTNG1+ thalamocortical axons deviated from their normal trajectory in white matter (WM) (arrowheads, **Fig. 2C**) and became markedly misrouted, including into tangential bundles through the upper cortical layers and toward the midline. Interestingly, NTNG1+ thalamocortical axons largely did not contribute to the radially-directed aberrant axons in cKO-E, which were revealed by pan-axonal marker L1CAM (arrows, **Fig. 2C**).

During normal circuit wiring, thalamocortical axons follow a precisely timed developmental path from thalamus to cortex. In ctrl E15.5 cortex, NTNG1+ thalamocortical axons had crossed the pallial-subpallial border (PSB), taken a trajectory in the intermediate zone (IZ), and reached the newly formed subplate (SP) positioned beneath the cortical plate (CP). Consistent with the “waiting period” (Kostovic and Rakic, 1984, 1990; Shatz and Luskin, 1986), thalamocortical axons at this age paused their ingrowth within the subplate zone and had not entered the cortical plate in ctrl (**Fig. 2D**). Remarkably, following cortical deletion of *Arid1a* in cKO-E, NTNG1+ thalamocortical axons prematurely invaded the cortical plate in cKO-E as aberrant bundles of axons (arrowheads, **Fig. 2D**). By E16.5, there was an abundance of thalamocortical axons prematurely invading in the cortical plate in cKO-E (**Fig. 2E**). This bypassing of the waiting period by thalamocortical axons was remarkably reminiscent of a characteristic consequence of subplate ablation (Ghosh et al., 1990; Ghosh and Shatz, 1993). In addition, in cKO-E, NTNG1+ axons did not cross the pallial-subpallial border (PSB) along the normal path. Instead, they formed a dense aberrant bundle parallel to the PSB (arrow, **Fig. 2D**) and ultimately entered the pallium more dorsally. Notably, similar to the bypassing of the waiting period, disrupted PSB crossing of thalamocortical axons has also been shown to be a consequence of disrupted subplate function (Chen et al., 2012; Magnani et al., 2013; Shinmyo et al., 2015). Together, the misrouting of thalamocortical axons following cortex-specific deletion of *Arid1a* in cKO-E revealed a non-cell autonomous function of *Arid1a* in axon guidance. Moreover, premature invasion of the cortical plate by thalamocortical axons and disruption in their crossing of the PSB implicated a potential role of subplate in *Arid1a* mutant phenotypes.

Correct callosal axon targeting following sparse deletion of *Arid1a*

The misrouting of thalamocortical axons in cKO-E revealed a non-cell autonomous role for *Arid1a* in axon pathfinding. To determine whether the misrouting of intracortical axons was also the result of disrupted non-cell autonomous *Arid1a* function, we sought to sparsely delete *Arid1a* from a subset of upper-layer cortical neurons by *in utero* electroporation (IUE), which would enable us to assess the cell autonomous consequences of *Arid1a* deletion within an *Arid1a*-expressing cortex. We generated a self-excising, self-reporting *Cre*-recombinase construct (CAG-sxiCre-EGFP) that would express Cre, and upon Cre recombination, simultaneously excise *Cre* and turn on EGFP reporter expression (**Fig. S3A**). The sxiCre

construct was transfected into embryonic cortex by IUE, where plasmid DNA was injected through the uterus, into the lateral ventricles of developing embryos, and transfected into NPCs by applying an electrical current (Kwan et al., 2008). We performed IUE at E14.5 to target NPCs during the genesis of upper-layer neurons, which form the majority of callosal axons, and analyzed the transfected brains at P0. To directly compare the effects of sparse versus widespread loss of *Arid1a*, we used ctrl, cKO-E, and *Arid1a*$^{fl/fl}$ (without genetic Cre) littermates for IUE. The presence or absence of ARID1A in EGFP+ electroporated cells was determined by ARID1A immunostaining and quantified (**Fig. S3B**). In P0 ctrl, electroporated neurons, all of which expressed ARID1A, migrated to the upper cortical layers and projected EGFP+ axons into the corpus callosum that reached the contralateral cortex (**Fig. 3A-C**). Following broad, genetic deletion of *Arid1a* in cKO-E, electroporated neurons migrated correctly to the upper layers, but failed to project axons across the corpus callosum; none of the EGFP-labeled axons reached the contralateral hemisphere (**Fig. 3D-F**). This absence was accompanied by aberrant radially-directed axons originating from transfected neurons (**Fig. S3C**), which was consistent with our axon analyses by genetic anterograde tracing using Cre-dependent *ROSA*^{mTmG} (**Fig. 1F**). Following sparse *Arid1a* deletion by sxiCre IUE in *Arid1a*$^{fl/fl}$ mice (**Fig. 3G**), electorporated neurons migrated correctly to the upper layers in a manner similar to ctrl (**Fig. 3H**). Remarkably, despite the absence of ARID1A (**Figs. 3G** and **S3B**), these neurons abundantly extended EGFP+ axon projections into the corpus callosum and correctly targeted contralateral cortex in a manner that was indistinguishable from ctrl (**Fig. 3I**), in stark contrast to widespread *Arid1a* deletion in cKO-E mice (**Fig. 3F**). Together, our results provided strong support that the callosal and thalamocortical axon pathfinding defects in cKO-E were non-cell autonomous consequences of broad cortical *Arid1a* deletion.

Selective disruption of subplate neuron gene expression following *Arid1a* deletion

To gain mechanistic insights into the axon guidance role of *Arid1a*, we sought to explore its molecular functions. As a chromatin remodeler, ARID1A mediates transcriptional regulation (Alver et al., 2017; Kelso et al., 2017; Mathur et al., 2017; Trizzino et al., 2018). To determine the potential influence of *Arid1a* deletion on gene expression, we analyzed the transcriptomes of cKO-E and littermate control cortices at E15.5, a developmental stage when intracortical and thalamocortical axons undergo extension and pathfinding to reach their targets (Anton-Bolanos et al., 2018; Auladell et al., 2000; Ozaki and Wahlsten, 1992). We generated libraries for unique molecular identifier (UMI) RNA-seq using Click-seq (Routh et al., 2015) from E15.5 cKO-E and littermate control cortices (ctrl: n=6, cKO-E: n=6 animals). In UMI RNA-seq, the tagging of each individual cDNA molecule by Click addition of a UMI barcode enables de-duplication of PCR-amplified reads post-sequencing (Keil et al., 2020; Shi et al., 2019). The wide dynamic range of UMI RNA-seq was confirmed by our analysis of spike-in ERCC standards (**Fig. S4A**). Differential gene expression was analyzed using edgeR (Robinson et al., 2010), which revealed significant differential expression of 103 annotated genes in cKO-E compared to ctrl with a stringent false discovery rate (FDR) of <0.01 (**Fig. 4A**). Gene expression changes based on UMI RNA-seq were quantitatively validated by digital droplet (dd)RT-PCR for two significantly downregulated genes (*Tle4*, *Zfpm2*) and two genes without significant changes (*Lhx2*, *Tbr1*) (**Fig. S4B**).

Arid1a has been reported to play a role in increasing or maintaining transcriptional activity by controlling the accessibility of enhancers (Mathur et al., 2017). Our result that a large majority of differentially expressed genes was significantly downregulated in cKO-E (91/103) is consistent with this role of *Arid1a*. To determine whether the axon defects in cKO-E may be associated with reduced expression of axon extension or axon guidance genes, we intersected the 91 significantly downregulated genes with 138 known axon extension genes (GO:0048675) and 253 known axon guidance genes (GO:0007411). This analysis (**Fig. S4C**) revealed a single downregulated axon extension gene (*Myo5b*) and a single downregulated guidance gene (*Ablim1*) in cKO-E. Hypergeometric analyses showed that neither group was significantly overrepresented (P_{hyper} =

0.36 and 0.34, respectively), suggesting that overall, the expression of known axon extension and guidance genes was not significantly altered in *Arid1a* cKO-E.

ARID1A is broadly, likely ubiquitously, expressed in brain development (**Fig. 1A**). Broadly expressed chromatin regulators, however, can mediate context- or cell type-dependent transcription. To determine whether gene expression from particular cortical cell types was preferentially affected in *Arid1a* cKO-E, we performed intersectional analysis with single cell RNA-seq (scRNA-seq) data from wildtype embryonic cortex (Yuzwa et al., 2017). Unsupervised hierarchical clustering of cKO-E downregulated genes revealed a cluster with 46/91 genes (cluster 1) that are highly co-expressed at the level of single cells (**Fig. 4B**), suggesting that this cluster of downregulated genes is normally expressed from one cell type. To validate this important finding, we performed intersection analysis using an orthogonal scRNA-seq dataset from wildtype E14.5 embryonic cortex (Loo et al., 2019). Unsupervised hierarchical clustering with this dataset revealed single-cell co-expression of 58/91 cKO-E downregulated genes (cluster A, **Fig. S4D**). Remarkably, each of the 46 genes in cluster 1 were also represented in cluster A. This complete overlap provided high confidence that the downregulated genes in cKO-E reflected selective disruption of a single cell type. To unbiasedly determine the identity of this putative cell type, we intersected the 46 cluster 1 genes with a rich spatiotemportal gene expression dataset covering over 1200 brain subregions (Sunkin et al., 2013) using Enrichr (Chen et al., 2013; Kuleshov et al., 2016). This revealed a statistically significant enrichment of genes selectively expressed in cortical layer 6b (**Fig. 4C**). Layer 6b is an alternative nomenclature for subplate. We next intersected cluster 1 genes with additional datasets orthogonal to the discovery data. We found significant over-representation of genes preferentially expressed in subplate based on cell-typed specific RNA-seq (Molyneaux et al., 2015) and analysis of gene expression in microdissected subplate (Oeschger et al., 2012) (**Fig. 4D**). E14.5 *in situ* hybridization data from the Genepaint consortium (Visel et al., 2004) and E15.5 EGFP transgene expression data from the GENSAT consortium (Gong et al., 2003) added further support that genes within cluster 1 are preferentially expressed in subplate neurons (**Fig. 4E**). Together, our analyses revealed a selective disruption of subplate neuron molecular identity following *Arid1a* deletion.

Consistent with disruption of subplate neuron gene expression in *Arid1a* cKO-E, anatomical development of subplate neurons was also altered. In P0 ctrl cortex, subplate neurons labeled by RBFOX3 were organized in a distinct, narrow band positioned just beneath the cortical plate (**Fig. 4F**). In cKO-E, however, there was an absence of a discrete and organized subplate layer; with subplate neurons dispersed in a radially thicker band. Quantification revealed significant subplate thickening in cKO-E (**Fig. 4G**). We further analyzed the expression of subplate marker CPLX3. In ctrl, CPLX3 specifically labeled neurons within a continuous, discrete subplate band (**Fig. 4H**). In cKO-E, the band of CPLX3-labeled subplate neurons was characterized by gaps (asterisks), and some were abnormally present in white matter. Moreover, CPLX3-labeled neurons were significantly more dispersed (**Fig. 4I**). Together, these data suggested that subplate neurons were anatomically disorganized in cKO-E. However, based on CPLX3 marker staining, subplate neurons were present in cKO-E cortex. This is consistent with our transcriptome data, in which we identified expression changes in a number of genes selectively expressed in subplate neurons, but not all of them, implicating the presence of subplate neurons with partially altered molecular identity in cKO-E. Together, our data supported that the anatomical development and cell type-dependent gene expression of subplate neurons were disrupted following *Arid1a* deletion.

Altered organization and morphogenesis of embryonic subplate neurons following *Arid1a* deletion

The selective alteration of subplate neuron molecular identity and non-cell autonomous misrouting of cortical axons in cKO-E suggested that *Arid1a* function in axon guidance may be centered on subplate neurons. Consistent with this possibility, subplate neurons are indispensable for the developmental wiring of cortical circuits; subplate ablation misroutes cortical axons and causes thalamocortical axons to prematurely

invade the cortical plate in a manner strikingly reminiscent of *Arid1a* cKO-E phenotypes (**Fig. 2**) (Ghosh et al., 1990; Ghosh and Shatz, 1992, 1993). Furthermore, disrupted subplate function has been shown to contribute to defects in thalamocortical axon crossing of the pallial-subpallial boundary and formation of cortical sensory maps (Chen et al., 2012; Kanold and Shatz, 2006; Magnani et al., 2013; Shinmyo et al., 2015) similar to those we found following *Arid1a* deletion (**Fig. 2**). We therefore sought to characterize the organization, morphology, axon projection, and extracellular matrix of subplate neurons in *Arid1a* cKO-E cortex.

Subplate mediates cortical axon pathfinding during embryonic ages. We thus assessed whether embryonic subplate organization was altered following *Arid1a* deletion. We first used immunostaining of TUBB3 (TUJ1), a marker of neurons and their processes that can be used to reveal the anatomical structure of embryonic cortical layers. In ctrl E14.5 cortex, TUBB3+ processes were horizontally organized in intermediate zone (IZ), subplate, and marginal zone (MZ), and radially organized in cortical plate (CP). In cKO-E, however, TUBB3-labeled axons became defasciculated in IZ, and aberrantly invaded the cortical plate diagonally (**Fig. 5A**). Analysis of MAP2, a somatodendritic marker of neurons that at this age preferentially labels subplate neurons, revealed a distinct horizontal organization of subplate neurons within a clearly delineated, continuous layer below the cortical plate in ctrl (**Fig. 5B**). Many MAP2-labeled neurons were co-labeled by NR4A2 (NURR1), a marker of subplate and L6 neurons. In cKO-E, however, we found abnormal clustering and cell-sparse gaps in MAP2- and NR4A2-labeled neurons in the presumptive subplate. Notably, misoriented MAP2-labeled dendrites aberrantly projected ventrally into intermediate zone in cKO-E (arrowheads, **Fig. 5B**). We further used the Tg(*Lpar1-EGFP*) transgenic allele, which expresses EGFP in a subset of subplate neurons (Gong et al., 2003; Hoerder-Suabedissen and Molnár, 2013). In E16.5 cKO-E cortex, Lpar1-EGFP-labeled subplate neurons were characterized by cell-sparse gaps (asterisks, **Fig. 5C**) and a few of them were aberrantly positioned in intermediate zone (arrows, **Fig. 5C**). Together, these data indicated a disorganization of subplate neurons in cKO-E, including abnormal clustering and cell-sparse gaps in the subplate layer and mispositioning of a small number of subplate neurons in the intermediate zone.

The aberrant clustering of neurons and misdirected dendrites suggested morphological disruption of subplate neurons in cKO-E. To analyze the morphology of single subplate neurons, we leveraged an *in vivo* genome editing method that targets the actin gene *Actb* for sparse, whole-cell cytoskeletal labeling. To do this, we used CRISPR-Cas9 to generate a targeted DNA double strand break at the C-terminus of the *Actb* coding region (Suzuki et al., 2016; Yao et al., 2017) and a homology-independent repair template containing sgRNA target sites flanking a 3xHA epitope tag (Keil et al., 2020). CRISPR-Cas9 cleavage of the repair construct would generate a short repair template without homology and NHEJ repair in the forward orientation would lead to in-frame expression of ACTB-3xHA. To perform the assay *in vivo*, we used *in utero* electroporation (IUE) to co-transfect CRISPR-Cas9, the repair template, and CAG-mTagBFP2 into cortical NPCs at E11.5, during the peak of subplate neuronogenesis (schematized in **Fig. 5D**). Analyzed at E16.5, CAG-mTagBFP2 revealed successful targeting of subplate neurons (**Fig. 5E**). In ctrl cortex, CAG-mTagBPF2-labeled neurons were organized in a narrow band positioned just beneath cortical plate. In cKO-E cortex, however, CAG-mTagBPF2-labeled neurons showed aberrant clustering reminiscent of MAP2 and Lpar1-EGFP labeling (**Fig. 5B** and **C**).

Next, we used anti-HA immunostaining to reveal the whole cell morphology of sparsely-labeled subplate neurons. Reconstruction of confocal z-stacks revealed a diversity of subplate neuron morphologies in ctrl cortex, including pyramidal, horizontal, and multipolar (**Fig. 5F** and **G**). Diverse subclasses in subplate neuron morphology have been previously documented (De Carlos and O'Leary, 1992; Hoerder-Suabedissen and Molnár, 2012; Luhmann et al., 2018; Molnar et al., 1998; Molnár et al., 1998), although embryonic subplate neuron morphologies have not been extensively characterized. In cKO-E cortex, the morphologies of subplate neurons were also diverse; however, many deviated from the morphological subclasses observed

in normal subplate. Notably, unlike subplate neurons, the morphology of newborn pyramidal neurons in cKO-E was indistinguishable from ctrl (**Fig. S5**). Thus, our data revealed cell-type dependent alterations in morphogenesis of subplate neurons.

Disrupted subplate neuron axon projection and extracellular matrix following *Arid1a* deletion

Subplate neurons are the first neurons to extend corticofugal axons. These early descending axons contribute to the guidance of thalamocortical ascending axons via co-fasciculation in a model known as the "handshake hypothesis" (Blakemore and Molnar, 1990; Molnar et al., 2012; Molnár and Blakemore, 1991; Molnár and Blakemore, 1995) (schematized in **Fig. 6A**). Subplate axons also guide thalamocortical axons across the pallial-subpallial boundary (Molnar et al., 2012). To visualize the extension of corticofugal axons from subplate neurons, we leveraged the Tg(*Golli-tau-EGFP*) transgenic mouse, which expresses EGFP fused with TAU(τ) specifically in subplate and L6 neurons (Jacobs et al., 2007; Piñon et al., 2009). In E15.5 ctrl cortex, an abundance of τEGFP-labeled axons had extended across the pallial-subpallial boundary. In the subpallium, these descending axons were closely apposed with NTNG1-labeled thalamocortical axons in a manner consistent with co-fasciculation (solid arrowheads, **Fig. 6B**). In contrast, in cKO-E cortex, innervation of the subpallium by τEGFP-labeled axons was severely attenuated and no co-fasciculation with NTNG1-labeled thalamocortical axons was found (open arrowheads, **Fig. 6B**). By E17.5, extensive co-fasciculation of τEGFP-labeled corticofugal axons and NTNG1-labeled thalamocortical axons was present in ctrl brain, but was largely absent from cKO-E (**Fig. 6C**). Concomitant with loss of co-fasciculation, NTNG1-labeled axons were unable to correctly traverse the pallial-subpallial boundary, entered the cortex via an aberrant dorsal path, became disorganized and defasiciculated in intermediate zone, and prematurely invaded cortical plate (**Fig. 2**). The misrouting of thalamocortical axons following loss of co-fasciculation with subplate axons is consistent with the model posited by the "handshake hypothesis" (Molnár et al., 1998).

Subplate neurons are rich in extracellular matrix (Judas et al., 2003; Kostovic et al., 2002; Kostović et al., 2019; Pearlman and Sheppard, 1996) and secreted molecules derived from subplate neurons are thought to signal the pathfinding of axons traversing the subplate zone (Hoerder-Suabedissen and Molnar, 2015; Kondo et al., 2015). Notably, during pathfinding, thalamocortical axons innervate the cortex via a white matter corridor delineated by chondroitin sulfate proteoglycan (CSPG), an extracellular matrix component richly present in the subplate zone (Bicknese et al., 1994; Sheppard et al., 1991). We analyzed the expression of CSPG in E15.5 and E16.5 ctrl and *Arid1a* cKO-E cortex. In ctrl, thalamocortical axons laterally traversed the embryonic cortex within a corridor neatly delineated by CSPG (**Fig. 6D** and **E**), which is consistent with previous studies (Bicknese et al., 1994). In cKO-E, however, CSPG expression was reduced and the CSPG corridor had collapsed (**Fig. 6D** and **E**). Concomitant with CSPG corridor disruption, thalamocortical axons were not confined within white matter, deviated from their normal trajectory, and prematurely invaded cortical plate (**Fig. 6D** and **E**). Together, our analyses revealed deficits in subplate neuron morphogenesis, subplate axon projections, and subplate extracellular matrix following *Arid1a* deletion.

Subplate-spared cortical plate deletion of *Arid1a* extensively corrected axon misrouting

Collectively, our data revealed *Arid1a* function in subplate neuron identity and development, and in non-cell autonomous guidance of cortical axons. To experimentally test the hypothesis that subplate neurons mediate the axon guidance function of *Arid1a*, we sought to determine whether *Arid1a* expression in subplate neurons was sufficient to support axon pathfinding from cortical neurons that lack *Arid1a*. To do this, we generated an *Arid1a* cKO using Tg(*hGFAP-Cre*) (Zhuo et al., 2001). Tg(*hGFAP-Cre*) mediates Cre recombination in cortical NPCs starting at E12.5, after the majority of subplate neurons have been generated. Therefore, *Arid1a* would be deleted from cortical plate neurons, whereas subplate neurons would be spared. This pattern of subplate-spared cortical deletion was confirmed by ARID1A immunostaining in these

conditional mutants (Tg[*hGFAP-Cre*];*Arid1a*$^{fl/fl}$, **cKO-hG**) (**Fig. 7A**). Importantly, Tg(*hGFAP-Cre*) mediated *Arid1a* deletion from the majority of L6 neurons (**Fig. S7A**), thus uncoupling the potential effects of subplate neurons from molecularly-related L6 neurons. In P0 cKO-hG, the sparing of subplate neurons from *Arid1a* deletion led to correct anatomical formation of the subplate band (**Fig. 7B** and **C**). Next, we analyzed cortical axon tracts using the Cre-dependent fluorescent reporter *ROSA*^{tdTomato} (Madisen et al., 2010) (**Fig. 7B**). Remarkably, in cKO-hG, tdTomato-labeled axons correctly entered the corpus callosum and successfully projected into contralateral cortex (**Fig. 7B** and **C**). Thus, *Arid1a* expression in subplate neurons in cKO-hG was sufficient for normal subplate organization and rescue of callosal agenesis observed in cKO-E. Furthermore, thalamocortical axon pathfinding was also remarkably rescued in cKO-hG. At P7, CO staining on flattened cortices revealed normal organization of barrel cortex in cKO-hG (**Fig. 7D**). Normal barrel development was confirmed by NTNG1 immunostaining on coronal sections, which revealed correct thalamocortical axon targeting of L4 whisker barrels in primary somatosensory cortex (**Fig. 7D**).

The correct targeting of callosal and thalamocortical axons in cKO-hG suggested that subplate neuron expression of *Arid1a* was sufficient for wiring of these tracts. To assess the wiring functions of the subplate in cKO-hG, we analyzed embryonic cortex. At E15.5, MAP2 immunostaining in cKO-hG revealed normal organization of subplate neurons indistinguishable from littermate ctrl (**Fig. 7E**). Importantly, NTNG1-labeled thalamocortical axons entered the cortex along a normal trajectory and without premature invasion of cortical plate (**Fig. 7E**). In addition, τEGFP-labeled corticofugal axons and NTNG1-labeled thalamocortical axons showed extensive co-fasciculation in cKO-hG (**Fig. 7F**). Furthermore, a CSPG corridor properly delineating the path of thalamocortical axons was present in cKO-hG (**Fig. 7G**), indicating that the subplate extracellular matrix was restored in cKO-hG. Therefore, despite a lack of ARID1A in cortical plate neurons, subplate expression of ARID1A in cKO-hG was sufficient for normal subplate organization, axon projections, and extracellular matrix, and extensively corrected the axon mistargeting phenotypes that followed pan-cortical *Arid1a* deletion in cKO-E. Together with our data from *Arid1a* cKO-E, our analysis of *Arid1a* cKO-hG enabled the dissection of cell and non-cell autonomous *Arid1a* functions. In subplate neurons, *Arid1a* cell autonomously established the transcription of subplate neuron identity genes, thus giving rise to correct subplate neuron morphology, subpallial axons, and extracellular matrix. By regulating the development of subplate neurons, *Arid1a* non-cell autonomously controlled the wiring of intracortical and thalamocortical connectivities via the axon guidance functions of the subplate. Thus, *Arid1a* played a key role in cortical circuit wiring centered on subplate neurons (schematized in **Fig. 8**).

DISCUSSION

Despite the central role of subplate neurons in cortical circuit assembly and their potential contribution to neurodevelopmental disorders (Hoerder-Suabedissen and Molnar, 2015; Serati et al., 2019), they are relatively understudied compared to their cortical plate counterparts. Molecular studies have largely focused on subplate-enriched genes (Hoerder-Suabedissen et al., 2013; Oeschger et al., 2012). Together, these studies have characterized molecular determinants of subplate neuron specification, migration, and axon development (Arai et al., 2019; Caviness, 1982; Han et al., 2011; Hevner et al., 2001; Kwan et al., 2008; Lai et al., 2008; Rakic et al., 2006; Ratie et al., 2019; Tiong et al., 2019), highlighting the complex genetic regulation required for subplate neuron development. The severe axon misrouting phenotypes of subplate ablation (Ghosh et al., 1990; Ghosh and Shatz, 1992, 1993), however, are not broadly recapitulated in these genetic mutants, precluding further mechanistic investigations into the circuit wiring functions of subplate neurons. Here, we leverage cortical *Arid1a* deletion, which shows axon misrouting defects strikingly reminiscent of subplate ablation, to gain molecular and functional insights into the non-cell autonomous mechanisms and tract-dependent functions of subplate neurons in assembly of cortical circuitry.

ARID1A is ubiquitously expressed during cortical development. Our findings, however, reveal an unexpectedly selective role for *Arid1a* in establishing the molecular identity and circuit wiring function of subplate neurons. Following deletion of *Arid1a* from cortical NPCs, callosal and thalamocortical axons are markedly misrouted in a manner phenotypically reminiscent of subplate ablation. Transcriptome analyses reveal selective dysregulation of subplate neuron-enriched gene transcription. Consistent with altered gene expression, subplate neuron organization, axon projections, morphogenesis, and extracellular matrix are each disrupted. Strikingly, subplate-spared cortical plate deletion of *Arid1a* restores subplate organization, connections, and extracellular matrix, and is sufficient to support correct axon pathfinding of cortical neurons that lack *Arid1a* and to guide proper formation of the thalamocortical tract. The axon guidance function of *Arid1a* in cortical development is therefore centered on the subplate – *Arid1a* cell type-selectively regulates the molecular identity and guidance function of subplate neurons, and thereby non-cell autonomously mediates the wiring of cortical connectivity.

Ablation studies from the 1990s first established a key role for the subplate in assembly of cortical connectivity (Ghosh et al., 1990; Ghosh and Shatz, 1992, 1993). This axon guidance role of subplate neurons is tract-dependent (De Carlos and O'Leary, 1992; Hoerder-Suabedissen and Molnar, 2015). In our study, we show that following *Arid1a* deletion, corticofugal axons innervate their targets largely without anatomical defect. In contrast, callosal and thalamocortical axons are broadly and severely misrouted. Thus, compared to the axon guidance function of subplate neurons, the role of *Arid1a* in wiring cortical connections is similarly tract-dependent.

Our cortical *Arid1a* deletion and previous experimental subplate ablation (Ghosh et al., 1990; Ghosh and Shatz, 1992, 1993; Kanold and Shatz, 2006) phenotypically converge on misrouted thalamocortical axons, which prematurely invade the cortical plate and ultimately fail to innervate their L4 targets with the correct topology. Furthermore, disruption of subplate function is known to cause defects in thalamocortical axon crossing of the pallial-subpallial boundary (Chen et al., 2012; Magnani et al., 2013; Shinmyo et al., 2015), an impairment we also observed following *Arid1a* deletion. Several aspects of subplate function may contribute to correct thalamocortical axon pathfinding (Garel and Rubenstein, 2004). First, the “handshake hypothesis” posits that close co-fasciculation between the earliest descending corticofugal axons, which originate from subplate neurons, and ascending thalamocortical axons is important for guidance of both tracts and formation of reciprocal connectivity (Blakemore and Molnar, 1990; Hevner et al., 2002; Molnar et al., 2012). Following *Arid1a* deletion in cKO-E, subplate corticofugal axons are markedly reduced, and their co-fasciculation with thalamocortical axons is lost. Consistent with the “handshake” hypothesis, thalamocortical axons are impaired in their crossing of the pallial-subpallial boundary, enter the cortex via an aberrant dorsal path, and become disorganized and defasciculated after entering the cortex in cKO-E. Second, the prenatal subplate is characterized by a remarkably rich extracellular matrix (Kostovic and Judas, 2010; Kostovic et al., 2002; Kostovic and Rakic, 1990; Pearlman and Sheppard, 1996). Extracellular matrix is required for axon guidance, by interacting with growth cones and enabling correct signaling by axon guidance molecules (Barros et al., 2011; Hoerder-Suabedissen and Molnar, 2015; Letourneau et al., 1994). During circuit formation, cortical afferent and efferent axons extend along a white matter corridor delineated by the extracellular matrix component CSPG (Bicknese et al., 1994). Following *Arid1a* deletion, CSPG expression is reduced and the corridor collapses. Concomitantly, thalamocortical axons become defasciculated in white matter and prematurely invade the cortical plate without waiting in the subplate, a phenotype strikingly reminiscent of subplate ablation (Ghosh and Shatz, 1993). The sparing of subplate neurons from *Arid1a* deletion (by using *Tg[hGFAP-Cre]*) restores both axon co-fasciculation and the CSPG corridor, and remarkably, is sufficient for correct thalamocortical axon pathfinding to their cortical targets. These data thus provide strong support that: 1) *Arid1a* function in thalamocortical tract formation is centered on subplate neurons; and 2) *Arid1a*-dependent subplate CSPG and axon co-fasciculation mediate thalamocortical axon pathfinding. Interestingly, corticothalamic axons from cortical plate neurons are largely intact following *Arid1a*

deletion, despite reduction and misrouting of subplate-thalamic axons. Thus, we do not find an *Arid1a*-dependent pioneering role for subplate axons in guiding corticothalamic axons from subsequent cortical plate neurons.

In addition to thalamocortical axons, intracortical axons are also markedly misrouted following *Arid1a* deletion in cKO-E. Unlike the better-known role of subplate neurons in thalamocortical axon guidance, subplate contribution to intracortical tract development is less established. Early studies suggested that subplate neurons pioneer corpus callosum formation by extending the first callosal axons (Antonini and Shatz, 1990; Chun et al., 1987; Hoerder-Suabedissen and Molnár, 2012; Koester and O'Leary, 1991; Ozaki and Wahlsten, 1992). Some subsequent studies, however, found this possibility to be unlikely (Koester and O'Leary, 1994; Ozaki and Wahlsten, 1998). In our study, we find that sparing *Arid1a* deletion from subplate neurons (by using Tg*[hGFAP-Cre]*) is sufficient to restore the corpus callosum, suggesting that subplate neurons play an *Arid1a*-dependent, non-cell autonomous role in callosal formation, although which aspects of subplate neuron function mediate this role remains to be determined.

One barrier to molecular study of subplate function is the lack of specific genetic access to prenatal subplate neurons during critical stages of circuit wiring. Although several published Cre lines show subplate neuron specificity, the onset of Cre expression occurs too late in these lines for study of circuit development (Hoerder-Suabedissen et al., 2018). Here, we directly compare conditional gene knockout by *Emx1*^{Cre}, which deletes *Arid1a* from NPCs that give rise to subplate neurons, and Tg(*hGFAP-Cre*), which deletes *Arid1a* from NPCs after subplate neurons have been generated. By sparing the subplate from deletion, this strategy enabled us to interrogate the sufficiency of *Arid1a* expression in subplate neurons. Importantly, Tg(*hGFAP-Cre*) mediates recombination from a majority of L6 neurons, thus enabling the potential effects of subplate neurons to be uncoupled from closely-related L6 neurons. Our use of Tg(*hGFAP-Cre*) thus highlights a genetic strategy for the study of subplate neuron gene function in cortical development.

Loss-of-function mutations in *ARID1A* are frequently found in human cancers and the molecular functions of ARID1A in cancer cells are being unraveled (Kadoch and Crabtree, 2015). ARID1A has been proposed to maintain transcriptional activity by recruiting EP300 acetyltransferase to enhancers (Alver et al., 2017; Mathur et al., 2017) or by controlling chromatin accessibility at enhancers (Kelso et al., 2017). A recent study, however, found that ARID1A depletion only modestly altered accessibility and proposed that ARID1A maintains RNA polymerase pausing near transcriptional start sites to enable robust transcription during homeostasis (Trizzino et al., 2018). In NPCs, we find that *Arid1a* deletion does not confer carcinogenic growth advantage. Instead, NPC deletion of *Arid1a* leads to a selective reduction in expression of a subset of neuronal genes. Despite ubiquitous ARID1A expression during cortical development, the effects of *Arid1a* deletion is surprisingly cell type-dependent: selectively disrupting subplate neuron molecular identity. A recent study showed that *Arid1b* expression following *Arid1a* depletion is sufficient to support BAF complex function (Trizzino et al., 2018). Thus, the expression of *Arid1b* may have attenuated the effects of *Arid1a* loss from cortical plate neurons.

Recent human genetic findings have convergently implicated altered chromatin regulation in multiple disorders of brain development (De Rubeis et al., 2014; Iwase and Martin, 2018; Sanders et al., 2015). These studies have identified *de novo* loss-of-function mutations in *ARID1A* in intellectual disability, ASD, and Coffin-Siris syndrome, a developmental disorder characterized by callosal agenesis (Kosho and Okamoto, 2014). Our study suggests that potential deficits in subplate neurons can contribute to altered brain development in these patients. Notably, like *ARID1A*, many of the chromatin genes implicated in neurodevelopmental disorders are also broadly or ubiquitously expressed (Ronan et al., 2013). How mutations in broadly expressed genes manifest as disorders of brain development remains largely mysterious. Here, we show a surprisingly cell type selective role for *Arid1a* in cortical development. Thus, it

is possible that other widely expressed chromatin regulators can have similar cell-type dependent functions. In addition, we discover an *Arid1a*-dependent, non-cell autonomous role for subplate neurons in the wiring of cortical circuits. Thus, non-cell autonomous mechanisms mediated by chromatin regulation may play an underappreciated role in neural circuit development and disorders thereof.

ACKNOWLEDGEMENTS
We thank members of the Kwan laboratory for discussions and comments on the manuscript, for critical reading of the manuscript, for scientific discussions, and colleagues in the MNI and Dept. of Human Genetics for insightful suggestions on this study. This work was supported by National Institutes of Health (R01 NS097525, R01 NS100156, and U01 MH106892 to K.Y.K., F31 NS110206 to D.Z.D., T32 GM007544 to O.H.F.), the Brain Research Foundation (BRFSG-2016-04 to K.Y.K.), March of Dimes Foundation (#5-FY15-33 to K.Y.K.), and Simons Foundation Autism Research Initiative (402213 and 324586 to K.Y.K.).

AUTHOR CONTRIBUTIONS
K.Y.K. conceived the study. D.Z.D. and K.Y.K designed experiments. D.Z.D., M.M.L., and A.S. performed experiments. D.Z.D., A.Q., Y.Q., O.H.F., and K.Y.K. analyzed data. D.Z.D. and K.Y.K. wrote the paper.

COMPETING INTERESTS
The authors declare no competing financial interests.

METHODS

Experimental Animals
The conditional-ready *Arid1a allele* and the *Emx1*^{Cre}, *ROSA*^{mTmG}, Tg(*hGFAP-Cre*), and *ROSA*^{tdTomato} mice were previously generated (Gao et al., 2008; Gorski et al., 2002; Madisen et al., 2010; Muzumdar et al., 2007; Zhuo et al., 2001) and obtained from the Jackson laboratory (Stock 027717, 005628, 007676, 004600, and 007914). The Tg(*Lpar1-EGFP*) mouse was previously generated (Gong et al., 2003) and purchased from the MMRRC (MMRRC:030171). The Tg(*Golli-tau-EGFP*) mouse (Jacobs et al., 2007) was a kind gift from Dr. Anthony Campagnoni. For timed pregnancies, the date of vaginal plug was considered embryonic day 0.5. Genotyping was performed using DreamTaq Green 2x Master Mix (Thermo Fisher) and genomic DNA isolated from toe or tail clips. Mice were maintained on a standard 12 hour day:night cycle with *ad libitum* access to food and water, and all experiments were carried out in compliance with ethical regulations for animal research. Our study protocol was reviewed and approved by the University of Michigan Institutional Animal Care & Use Committee.

Primers
<u>Genotyping primers:</u>
Arid1a^{fl} Forward: TGGGCAGGAAAGAGTAATGG
Arid1a^{fl} Reverse: AACACCACTTTCCCATAGGC
Cre Forward: TCGATGCAACGAGTGATGAG
Cre Reverse: TTCGGCTATACGTAACAGGG

<u>ddPCR primers and probes:</u>
Lhx2
Primer 1: GCATCTGACGTCTTGTCCAC
Primer 2: CTCACCAAGAGAGTCCTCCA
Probe: /56-FAM/TTTCCTGCC/Zen/GTAAAAGGTTGCGC/3IABkFQ/

Tbr1
Primer 1: CCCGTGTAGATCGTGTCATAG
Primer 2: AGACTCAGTTCATCGCTGTC
Probe: /56-FAM/TTTAGTTGT/Zen/GTAATATCCGTGTTCTGGTAGGC/3IABkFQ/

Tle4
Primer 1: ACTGACGTGAAAGGAGTATGC
Primer 2: AGCCTATGGAAGATCACCTGT
Probe: /56-FAM/ACATGCGAG/Zen/TGCCAGCAATACCT/3IABkFQ/

Zfpm2
Primer 1: TGGTTTGTCTGAATGGCTGT
Primer 2: GAAGACGTGGAGTTCTTTTGTAAC
Probe: /56-FAM/CATCTGATT/Zen/CTGCTGGCTCCTGGAT/3IABkFQ/

Srp72
Primer 1: CTCTCCTCATCATAGTCGTCCT
Primer 2: CTGAAGGAGCTTTATGGACAAGT
Probe: /5HEX/CCAAGCACT/Zen/CATCGTAGCGTTCCA/3IABkFQ/

Immunostaining and Imaging
Brains were isolated and fixed in 4% PFA overnight at 4°C with agitation, and embedded in 4% low-melting agarose for sectioning. Brains were vibratome-sectioned at 70µm using a Leica VT1000S or VT1200S. Free-floating sections were blocked and immunostained in blocking solution containing 5% donkey serum, 1% BSA, 0.1% glycine, 0.1% lysine, and 0.3% Triton X-100 (Triton X-100 was excluded from blocking solution when immunostaining for CSPG). Free-floating sections were incubated with primary antibodies overnight at 4°C followed by washing 3x5min in PBS and incubated with the corresponding fluorescent secondary antibodies and DAPI in blocking solution for 1h at RT. Following secondary antibody staining, sections were mounted with VECTASHIELD Antifade Mounting Medium (Vector Laboratories). Images were acquired using either an Olympus SZX16 dissecting scope with Olympus U-HGLGPS fluorescent source and Q-Capture Pro 7 software to operate a Q-imaging Regia 6000 camera, or using an Olympus Fluoview FV1000 confocal microscope with FV10-ASW software. Primary Antibodies: Rabbit anti-ARID1A (Abcam ab182560, 1:1000), Goat anti-SOX2 (Santa Cruz Biotechnology sc-17320, 1:250), Rabbit anti-TBR1 (Abcam ab31940, 1:250), Rat anti-BCL11B (Abcam ab18465, 1:500), Rabbit anti-LHX2 (Sigma-Aldrich ABE1402, 1:1000), Rat anti-L1CAM (Sigma-Aldrich MAB5272, 1:1000), Chicken anti-GFP (Abcam ab13970, 1:2000), Rabbit anti-GFP (Invitrogen A-11122, 1:1000), Goat anti-Netrin-G1a (R&D Systems AF1166, 1:100), Chicken anti-RBFOX3 (Sigma-Aldrich ABN91, 1:2000), Rabbit anti-CPLX3 (Synaptic Systems 122302, 1:1000), Mouse anti-TUBB3 (Covance MMS435-P, 1:1000), Rabbit anti-NR4A2 (Santa Cruz Biotechnology sc-990, 1:500), Chicken anti-MAP2 (Novus Biologicals NB300-213, 1:2000), Rabbit anti-tRFP (Evrogen AB233, 1:2000), Rat anti-HA (Sigma-Aldrich 1186723001, 1:1000), Mouse anti-Chondroitin Sulfate (Sigma-Aldrich C8035, 1:100). Secondary Antibodies: Donkey anti-Goat IgG (H+L), Alexa Fluor 488 AffiniPure (Jackson ImmunoResearch Labs Cat# 805-545-180, 1:250), Donkey anti-Rabbit IgG (H+L), Alexa Fluor 488 AffiniPure (Jackson ImmunoResearch Labs Cat# 711-545-152, 1:250), Donkey anti-Rat IgG (H+L), Alexa Fluor 488 AffiniPure (Jackson ImmunoResearch Labs Cat# 712-545-150, 1:250), Donkey anti-Chicken IgY (H+L), Alexa Fluor 488 Affinipure (Jackson ImmunoResearch Labs Cat# 703-545-155, 1:250), Donkey anti-Mouse IgG (H+L), Alexa Fluor 488 Affinipure (Jackson ImmunoResearch Labs Cat# 715-545-150, 1:250), Donkey anti-Mouse IgM, µ chain specific, Alexa Fluor 488 Affinipure (Jackson ImmunoResearch Labs Cat# 715-545-020, 1:250), Donkey anti-Goat IgG (H+L), Alexa Fluor Cy3 AffiniPure (Jackson ImmunoResearch Labs Cat# 705-165-147, 1:250), Donkey anti-Rabbit IgG (H+L), Alexa Fluor Cy3 AffiniPure (Jackson ImmunoResearch Labs

Cat# 711-165-152, 1:250), Donkey anti-Rat IgG (H+L), Alexa Fluor Cy3 AffiniPure (Jackson ImmunoResearch Labs Cat# 712-165-153, 1:250), Donkey anti-Chicken IgY (H+L), Alexa Fluor Cy3 Affinipure (Jackson ImmunoResearch Labs Cat# 703-165-155, 1:250), Donkey anti-Rabbit IgG (H+L), Alexa Fluor 647 AffiniPure (Jackson ImmunoResearch Labs Cat# 711-605-152, 1:250), Donkey anti-Chicken IgY (H+L), Alexa Fluor 647 AffiniPure (Jackson ImmunoResearch Labs Cat# 703-605-155, 1:250), Donkey anti-Rat IgG (H+L), Cy5 AffiniPure (Jackson ImmunoResearch Labs Cat# 712-175-153, 1:250).

Cytochrome Oxidase

Brains from P7 mutant and control mice were fixed for 4 h at room temperature in 4% PFA, and the cortices were dissected, flattened between two glass slides, and fixed overnight at 4°C. Following fixation, flattened cortices were sectioned on a vibratome at 150µm. Sections were incubated at 37°C overnight in a solution containing 4 g sucrose, 50 mg DAB, 15 mg cytochrome C per 100 mL of PBS. When staining was complete, sections were washed with PBS, mounted onto slides, and imaged with an Olympus SZX16 dissecting scope.

Plasmid constructs

For CAG-sxiCre-EGFP, iCre sequence interrupted by a chimeric intron, followed by polyA, and flanked by loxP sites was placed immediately downstream of the CAG promoter. EGFP, WPRE, and polyA were inserted following the iCre/loxP cassette so that Cre expression would lead to self-excision and EGFP expression. CAG-mTagBFP2 was generated by subcloning mTagBFP2 from mTagBFP2-Lifeact-7 (a gift from Michael Davidson, Addgene Plasmid #54602) (Subach et al., 2011) into pCAGEN (a gift from Connie Cepko, Addgene Plasmid #11160) (Matsuda and Cepko, 2004). To make eSpCas9opt1.1-Actb_gRNA (Keil et al., 2020), a gRNA sequence targeting the c-terminus of the *Actb* coding sequence (5′-AGTCCGCCTAGAAGCACTTG) was cloned into eSpCas9Opt1.1, which expresses enhanced-specificity Cas9 and an optimized gRNA scaffold. To construct Actb_NHEJ_3xHA (Keil et al., 2020), tandem HA tag sequences were cloned between 2 *Actb* gRNA recognition sequences, to enable 3xHA insertion into the *Actb* gene following cutting of the endogenous gene and the plasmid by Cas9.

***In utero* electroporation**

In utero electroporation was performed at E14.5 for sparse deletion of *Arid1a* or E11.5 for whole-cell morphology of subplate neurons, based on observation of a vaginal plug, for sparse deletion of *Arid1a* from upper layer neurons. A micropipette filled with either 1.5 µg/µL CAG-sxiCre-EGFP for sparse deletion, or with a mix of Actb_NHEJ_3xHA, eSpCas9opt1.1-Actb_gRNA, and CAG-mTagBFP2 each at 1 µg/µL for subplate neuron morphology, was inserted into the lateral ventricle and a World Precision Instruments Micro4 MicroSyringe Pump Controller was used to regulate the injection. A BTX Harvard Apparatus ECM 830 power supply was used to deliver five 45 millisecond, 27 volt pulses at 950 millisecond intervals via electroporation paddles to direct the plasmid into cells of the VZ. Electroporated brains were dissected and immunostained at P0 for ARID1A sparse deletion or at E16.5 for subplate neuron morphology.

RNA purification and droplet digital PCR (ddPCR)

Neocortical tissue was microdissected from E15.5 mice. RNA was isolated by resuspending the tissue in TRIzol, homogenizing with metal beads in a bullet blender, isolating the aqueous phase following addition of chloroform and centrifugation for 15 min at >20,000g at 4°C, and eluting purified RNA with DNase/RNase-free water from a Zymo Research Zymo-Spin IC column. Purified RNA was quantified using a Qubit fluorometer. 1µg of RNA was reverse transcribed using SuperScript II (Invitrogen). Probe sets (PrimeTime qPCR Probe Assays) from Integrated DNA Technologies were utilized with diluted cDNA and the QX200 Droplet Digital PCR System (Bio-Rad) for gene expression level analyses. The ddPCR reaction mixture contained template cDNA, 2xddPCR Supermix (No dUTP) (Bio-Rad), target probes with HEX fluorescence, and control probe against the house-keeping gene *Srp72* with FAM fluorescence. Droplets were generated

with the QX200 droplet generator (Bio-Rad), thermocycled, and analyzed using the QX200 droplet reader (Bio-Rad).

ClickSeq

RNA-seq libraries were generated by Click-Seq (Routh et al., 2015) from 600 ng of purified neocortical RNA. Ribosomal RNA was removed from total RNA using NEBNext rRNA Depletion Kit (NEB). ERCC RNA spike-in was included for library quality assessment (Thermo Fisher). Superscript II (Thermo Fisher) was used for reverse transcription with 1:30 5 mM AzdNTP:dNTP and 3′ Genomic Adapter-6N RT primer (GTGACTGGAGTTCAGACGTGTGCTCTTCCGATCTNNNNNN). RNaseH treatment was used to remove RNA template and DNA was purified with DNA Clean and Concentrator Kit (Zymo Research). Azido-terminated cDNA was combined with the click adaptor oligo (/5Hexynyl/NNNNNNNNAGATCGGAAGAGCGTCGTGTAGGGAAAGAGTGTAGATCTCGGTGGTCGCCGTATCATT) and click reaction was catalyzed by addition of ascorbic acid and Cu^{2+}, with subsequent purification with DNA Clean and Concentrator Kit. Amplification of the library was accomplished using the Illumina universal primer (AATGATACGGCGACCACCGAG) and Illumina indexing primer (CAAGCAGAAGACGGCATACGAGATNNNNNNGTGACTGGAGTTCAGACGTGT) and the manufacturer's protocols from the 2× One Taq Hot Start Mastermix (NEB). To enrich for amplification products larger than 200 bp, PCR products were purified using Ampure XP (Beckman) magnetic beads at 1.25× ratio. Libraries were analyzed on TapeStation (Agilent) for appropriate quality and distribution and were sequenced at the University of Michigan sequencing core on the Illumina NextSeq 550 platform (75 cycle, high output).

RNA sequencing data analysis

RNA-seq data were subject to quality-control check using FastQC v0.11.5 (https://www.bioinformatics.babraham.ac.uk/projects/download.html#fastqc). Adapters were trimmed using cutadapt version 1.13 (http://cutadapt.readthedocs.io/en/stable/guide.html). Processed reads were aligned to GENCODE GRCm38/mm10 reference genome (https://www.gencodegenes.org/mouse_releases/current.html) with STAR (Dobin et al., 2013) (v2.5.2a) and deduplicated according to UMI using UMI-tools (Smith et al., 2017) (v0.5.3). Read counts were obtained with htseq-count (v0.6.1p1) with intersection-nonempty mode (Anders et al., 2015). Differential expression was determined with edgeR (Robinson et al., 2010). The *P* value was calculated with likelihood ratio tests and the adjusted *P* value for multiple tested was calculated using the Benjamini-Hochberg procedure, which controls false discovery rate (FDR).

Single cell RNA-seq intersectional analysis

Single cell RNA-seq data were obtained (Loo et al., 2019; Yuzwa et al., 2017). To ensure consistency between methods, unclustered data were clustered using standard t-SNE cell-based clustering (Pedregosa et al., 2011). Raw counts were normalized with K-nearest neighbor smoothing and a Freeman-Tukey transform to improve the signal-to-noise ratio (Wagner et al., 2018). Pearson product-moment correlation coefficients for gene expression were calculated using NumPy (Harris et al., 2020) and plotted using seaborn (Waskom and seaborn development team, 2020).

Image data analysis

Age- and spatially-matched images of mutant and control mice were processed in ImageJ and Adobe Photoshop. Quantification was performed in ImageJ.

Statistical analysis

Statistical analyses were performed in GraphPad Prism 8 (GraphPad Software). Values were compared using a two-tailed, unpaired Student's *t* test or ANOVA with Tukey's post hoc test. A *P* value of < 0.05 was considered statistically significant unless otherwise indicated.

REFERENCES

Allendoerfer, K.L., and Shatz, C.J. (1994). The subplate, a transient neocortical structure: its role in the development of connections between thalamus and cortex. Annu Rev Neurosci *17*, 185-218.

Alver, B.H., Kim, K.H., Lu, P., Wang, X., Manchester, H.E., Wang, W., Haswell, J.R., Park, P.J., and Roberts, C.W. (2017). The SWI/SNF chromatin remodelling complex is required for maintenance of lineage specific enhancers. Nat Commun *8*, 14648.

Anders, S., Pyl, P.T., and Huber, W. (2015). HTSeq-a Python framework to work with high-throughput sequencing data. Bioinformatics *31*, 166-169.

Anton-Bolanos, N., Espinosa, A., and Lopez-Bendito, G. (2018). Developmental interactions between thalamus and cortex: a true love reciprocal story. Curr Opin Neurobiol *52*, 33-41.

Antonini, A., and Shatz, C.J. (1990). Relation Between Putative Transmitter Phenotypes and Connectivity of Subplate Neurons During Cerebral Cortical Development. Eur J Neurosci *2*, 744-761.

Arai, Y., Cwetsch, A.W., Coppola, E., Cipriani, S., Nishihara, H., Kanki, H., Saillour, Y., Freret-Hodara, B., Dutriaux, A., Okada, N.*, et al.* (2019). Evolutionary Gain of Dbx1 Expression Drives Subplate Identity in the Cerebral Cortex. Cell Rep *29*, 645-658.e645.

Auladell, C., Perez-Sust, P., Super, H., and Soriano, E. (2000). The early development of thalamocortical and corticothalamic projections in the mouse. Anat Embryol (Berl) *201*, 169-179.

Barros, C.S., Franco, S.J., and Muller, U. (2011). Extracellular matrix: functions in the nervous system. Cold Spring Harb Perspect Biol *3*, a005108.

Bicknese, A.R., Sheppard, A.M., O'Leary, D.D., and Pearlman, A.L. (1994). Thalamocortical axons extend along a chondroitin sulfate proteoglycan-enriched pathway coincident with the neocortical subplate and distinct from the efferent path. J Neurosci *14*, 3500-3510.

Blakemore, C., and Molnar, Z. (1990). Factors involved in the establishment of specific interconnections between thalamus and cerebral cortex. Cold Spring Harb Symp Quant Biol *55*, 491-504.

Caviness, V.S., Jr. (1982). Neocortical histogenesis in normal and reeler mice: a developmental study based upon [3H]thymidine autoradiography. Brain Res *256*, 293-302.

Chen, E.Y., Tan, C.M., Kou, Y., Duan, Q., Wang, Z., Meirelles, G.V., Clark, N.R., and Ma'ayan, A. (2013). Enrichr: interactive and collaborative HTML5 gene list enrichment analysis tool. BMC Bioinformatics *14*, 128.

Chen, Y., Magnani, D., Theil, T., Pratt, T., and Price, D.J. (2012). Evidence that descending cortical axons are essential for thalamocortical axons to cross the pallial-subpallial boundary in the embryonic forebrain. PLoS One *7*, e33105.

Chun, J.J., Nakamura, M.J., and Shatz, C.J. (1987). Transient cells of the developing mammalian telencephalon are peptide-immunoreactive neurons. Nature *325*, 617-620.

Consortium, E.P. (2012). An integrated encyclopedia of DNA elements in the human genome. Nature *489*, 57-74.

Consortium, G. (2015). Human genomics. The Genotype-Tissue Expression (GTEx) pilot analysis: multitissue gene regulation in humans. Science *348*, 648-660.

De Carlos, J.A., and O'Leary, D.D. (1992). Growth and targeting of subplate axons and establishment of major cortical pathways. J Neurosci *12*, 1194-1211.

De Rubeis, S., He, X., Goldberg, A.P., Poultney, C.S., Samocha, K., Ercument Cicek, A., Kou, Y., Liu, L., Fromer, M., Walker, S.*, et al.* (2014). Synaptic, transcriptional and chromatin genes disrupted in autism. Nature *515*, 209-215.

Dobin, A., Davis, C.A., Schlesinger, F., Drenkow, J., Zaleski, C., Jha, S., Batut, P., Chaisson, M., and Gingeras, T.R. (2013). STAR: ultrafast universal RNA-seq aligner. Bioinformatics *29*, 15-21.

Flores-Alcantar, A., Gonzalez-Sandoval, A., Escalante-Alcalde, D., and Lomeli, H. (2011). Dynamics of expression of ARID1A and ARID1B subunits in mouse embryos and in cells during the cell cycle. Cell Tissue Res *345*, 137-148.

Friauf, E., McConnell, S.K., and Shatz, C.J. (1990). Functional synaptic circuits in the subplate during fetal and early postnatal development of cat visual cortex. J Neurosci *10*, 2601-2613.

Gao, X., Tate, P., Hu, P., Tjian, R., Skarnes, W.C., and Wang, Z. (2008). ES cell pluripotency and germ-layer formation require the SWI/SNF chromatin remodeling component BAF250a. Proc Natl Acad Sci U S A *105*, 6656-6661.

Garel, S., and Rubenstein, J.L. (2004). Intermediate targets in formation of topographic projections: inputs from the thalamocortical system. Trends Neurosci *27*, 533-539.

Ghosh, A., Antonini, A., McConnell, S.K., and Shatz, C.J. (1990). Requirement for subplate neurons in the formation of thalamocortical connections. Nature *347*, 179-181.

Ghosh, A., and Shatz, C.J. (1992). Involvement of subplate neurons in the formation of ocular dominance columns. Science *255*, 1441-1443.

Ghosh, A., and Shatz, C.J. (1993). A role for subplate neurons in the patterning of connections from thalamus to neocortex. Development *117*, 1031-1047.

Gong, S., Zheng, C., Doughty, M., Losos, K., Didkovsky, N., Schambra, U., Nowak, N., Joyner, A., Leblanc, G., Hatten, M.*, et al.* (2003). A gene expression atlas of the central nervous system based on bacterial artificial chromosomes. Nature *425*, 917-925.

Gorski, J.A., Talley, T., Qiu, M., Puelles, L., Rubenstein, J.L., and Jones, K.R. (2002). Cortical excitatory neurons and glia, but not GABAergic neurons, are produced in the Emx1-expressing lineage. J Neurosci *22*, 6309-6314.

Han, W., Kwan, K.Y., Shim, S., Lam, M.M., Shin, Y., Xu, X., Zhu, Y., Li, M., and Sestan, N. (2011). TBR1 directly represses Fezf2 to control the laminar origin and development of the corticospinal tract. Proc Natl Acad Sci U S A *108*, 3041-3046.

Harris, C.R., Millman, K.J., van der Walt, S.J., Gommers, R., Virtanen, P., Cournapeau, D., Wieser, E., Taylor, J., Berg, S., and Smith, N.J. (2020). Array programming with NumPy. Nature *585*, 357-362.

Hevner, R., Shi, L., Justice, N., Hsueh, Y., Sheng, M., Smiga, S., Bulfone, A., Goffinet, A., Campagnoni, A., and Rubenstein, J. (2001). Tbr1 regulates differentiation of the preplate and layer 6. Neuron *29*, 353-366.

Hevner, R.F., Miyashita-Lin, E., and Rubenstein, J.L. (2002). Cortical and thalamic axon pathfinding defects in Tbr1, Gbx2, and Pax6 mutant mice: evidence that cortical and thalamic axons interact and guide each other. J Comp Neurol *447*, 8-17.

Ho, L., and Crabtree, G.R. (2010). Chromatin remodelling during development. Nature *463*, 474-484.

Hodges, C., Kirkland, J.G., and Crabtree, G.R. (2016). The Many Roles of BAF (mSWI/SNF) and PBAF Complexes in Cancer. Cold Spring Harb Perspect Med *6*.

Hoerder-Suabedissen, A., Hayashi, S., Upton, L., Nolan, Z., Casas-Torremocha, D., Grant, E., Viswanathan, S., Kanold, P.O., Clasca, F., Kim, Y.*, et al.* (2018). Subset of Cortical Layer 6b Neurons Selectively Innervates Higher Order Thalamic Nuclei in Mice. Cereb Cortex *28*, 1882-1897.

Hoerder-Suabedissen, A., and Molnar, Z. (2015). Development, evolution and pathology of neocortical subplate neurons. Nat Rev Neurosci *16*, 133-146.

Hoerder-Suabedissen, A., and Molnár, Z. (2012). Morphology of mouse subplate cells with identified projection targets changes with age. J Comp Neurol *520*, 174-185.

Hoerder-Suabedissen, A., and Molnár, Z. (2013). Molecular diversity of early-born subplate neurons. Cereb Cortex *23*, 1473-1483.

Hoerder-Suabedissen, A., Oeschger, F.M., Krishnan, M.L., Belgard, T.G., Wang, W.Z., Lee, S., Webber, C., Petretto, E., Edwards, A.D., and Molnár, Z. (2013). Expression profiling of mouse subplate reveals a dynamic gene network and disease association with autism and schizophrenia. Proc Natl Acad Sci U S A *110*, 3555-3560.

Iwase, S., and Martin, D.M. (2018). Chromatin in nervous system development and disease. Mol Cell Neurosci *87*, 1-3.

Jacobs, E., Campagnoni, C., Kampf, K., Reyes, S., Kalra, V., Handley, V., Xie, Y., Hong-Hu, Y., Spreur, V., Fisher, R.*, et al.* (2007). Visualization of corticofugal projections during early cortical development in a tau-GFP-transgenic mouse. Eur J Neurosci *25*, 17-30.

Judas, M., Milosević, N.J., Rasin, M.R., Heffer-Lauc, M., and Kostović, I. (2003). Complex patterns and simple architects: molecular guidance cues for developing axonal pathways in the telencephalon. Prog Mol Subcell Biol *32*, 1-32.

Kadoch, C., and Crabtree, G.R. (2015). Mammalian SWI/SNF chromatin remodeling complexes and cancer: Mechanistic insights gained from human genomics. Sci Adv *1*, e1500447.

Kang, H.J., Kawasawa, Y.I., Cheng, F., Zhu, Y., Xu, X., Li, M., Sousa, A.M., Pletikos, M., Meyer, K.A., Sedmak, G.*, et al.* (2011). Spatio-temporal transcriptome of the human brain. Nature *478*, 483-489.

Kanold, P.O., and Luhmann, H.J. (2010). The subplate and early cortical circuits. Annu Rev Neurosci *33*, 23-48.

Kanold, P.O., and Shatz, C.J. (2006). Subplate neurons regulate maturation of cortical inhibition and outcome of ocular dominance plasticity. Neuron *51*, 627-638.

Keil, J.M., Doyle, D.J., Qalieh, A., Lam, M.M., Funk, O.H., Qalieh, Y., Shi, L., Mohan, N., Sorel, A., and Kwan, K.Y. (2020). Symmetric neural progenitor divisions require chromatin-mediated homologous recombination DNA repair by Ino80. Nat Commun *in press*.

Kelso, T.W.R., Porter, D.K., Amaral, M.L., Shokhirev, M.N., Benner, C., and Hargreaves, D.C. (2017). Chromatin accessibility underlies synthetic lethality of SWI/SNF subunits in ARID1A-mutant cancers. Elife *6*.

Koester, S.E., and O'Leary, D.D. (1991). Subplate cells in medial cortex send the first axons across the corpus callosum. Soc Neurosci Abstr *15*.

Koester, S.E., and O'Leary, D.D. (1994). Axons of early generated neurons in cingulate cortex pioneer the corpus callosum. J Neurosci *14*, 6608-6620.

Kondo, S., Al-Hasani, H., Hoerder-Suabedissen, A., Wang, W.Z., and Molnár, Z. (2015). Secretory function in subplate neurons during cortical development. Front Neurosci *9*, 100.

Kosho, T., and Okamoto, N. (2014). Genotype-phenotype correlation of Coffin-Siris syndrome caused by mutations in SMARCB1, SMARCA4, SMARCE1, and ARID1A. Am J Med Genet C Semin Med Genet *166c*, 262-275.

Kostovic, I., and Judas, M. (2010). The development of the subplate and thalamocortical connections in the human foetal brain. Acta Paediatr *99*, 1119-1127.

Kostovic, I., Judas, M., Rados, M., and Hrabac, P. (2002). Laminar organization of the human fetal cerebrum revealed by histochemical markers and magnetic resonance imaging. Cereb Cortex *12*, 536-544.

Kostovic, I., and Rakic, P. (1984). Development of prestriate visual projections in the monkey and human fetal cerebrum revealed by transient cholinesterase staining. J Neurosci *4*, 25-42.

Kostovic, I., and Rakic, P. (1990). Developmental history of the transient subplate zone in the visual and somatosensory cortex of the macaque monkey and human brain. J Comp Neurol *297*, 441-470.

Kostović, I., Išasegi, I., and Krsnik, Ž. (2019). Sublaminar organization of the human subplate: developmental changes in the distribution of neurons, glia, growing axons and extracellular matrix. J Anat *235*, 481-506.

Kuleshov, M.V., Jones, M.R., Rouillard, A.D., Fernandez, N.F., Duan, Q., Wang, Z., Koplev, S., Jenkins, S.L., Jagodnik, K.M., Lachmann, A.*, et al.* (2016). Enrichr: a comprehensive gene set enrichment analysis web server 2016 update. Nucleic Acids Res *44*, W90-97.

Kwan, K.Y., Lam, M.M., Krsnik, Z., Kawasawa, Y.I., Lefebvre, V., and Sestan, N. (2008). SOX5 postmitotically regulates migration, postmigratory differentiation, and projections of subplate and deep-layer neocortical neurons. Proc Natl Acad Sci U S A *105*, 16021-16026.

Kwan, K.Y., Sestan, N., and Anton, E.S. (2012). Transcriptional co-regulation of neuronal migration and laminar identity in the neocortex. Development *139*, 1535-1546.

Lai, T., Jabaudon, D., Molyneaux, B., Azim, E., Arlotta, P., Menezes, J., and Macklis, J. (2008). SOX5 Controls the Sequential Generation of Distinct Corticofugal Neuron Subtypes. Neuron *57*, 232-247.

Letourneau, P.C., Condic, M.L., and Snow, D.M. (1994). Interactions of developing neurons with the extracellular matrix. J Neurosci *14*, 915-928.

Loo, L., Simon, J.M., Xing, L., McCoy, E.S., Niehaus, J.K., Guo, J., Anton, E.S., and Zylka, M.J. (2019). Single-cell transcriptomic analysis of mouse neocortical development. Nat Commun *10*, 134.

Luhmann, H.J., Kirischuk, S., and Kilb, W. (2018). The Superior Function of the Subplate in Early Neocortical Development. Front Neuroanat *12*, 97.

Madisen, L., Zwingman, T.A., Sunkin, S.M., Oh, S.W., Zariwala, H.A., Gu, H., Ng, L.L., Palmiter, R.D., Hawrylycz, M.J., Jones, A.R.*, et al.* (2010). A robust and high-throughput Cre reporting and characterization system for the whole mouse brain. Nat Neurosci *13*, 133-140.

Magnani, D., Hasenpusch-Theil, K., and Theil, T. (2013). Gli3 controls subplate formation and growth of cortical axons. Cereb Cortex *23*, 2542-2551.

Mathur, R., Alver, B.H., San Roman, A.K., Wilson, B.G., Wang, X., Agoston, A.T., Park, P.J., Shivdasani, R.A., and Roberts, C.W. (2017). ARID1A loss impairs enhancer-mediated gene regulation and drives colon cancer in mice. Nat Genet *49*, 296-302.

Matsuda, T., and Cepko, C.L. (2004). Electroporation and RNA interference in the rodent retina in vivo and in vitro. Proc Natl Acad Sci U S A *101*, 16-22.

McConnell, S., Ghosh, A., and Shatz, C. (1989). Subplate neurons pioneer the first axon pathway from the cerebral cortex. Science *245*, 978-982.

McConnell, S., Ghosh, A., and Shatz, C. (1994). Subplate pioneers and the formation of descending connections from cerebral cortex. J Neurosci *14*, 1892-1907.

Molnar, Z., Adams, R., and Blakemore, C. (1998). Mechanisms underlying the early establishment of thalamocortical connections in the rat. J Neurosci *18*, 5723-5745.

Molnar, Z., and Blakemore, C. (1995). How do thalamic axons find their way to the cortex? Trends Neurosci *18*, 389-397.

Molnar, Z., Garel, S., Lopez-Bendito, G., Maness, P., and Price, D.J. (2012). Mechanisms controlling the guidance of thalamocortical axons through the embryonic forebrain. Eur J Neurosci *35*, 1573-1585.

Molnár, Z., Adams, R., Goffinet, A.M., and Blakemore, C. (1998). The role of the first postmitotic cortical cells in the development of thalamocortical innervation in the reeler mouse. J Neurosci *18*, 5746-5765.

Molnár, Z., and Blakemore, C. (1991). Lack of regional specificity for connections formed between thalamus and cortex in coculture. Nature *351*, 475-477.

Molnár, Z., and Blakemore, C. (1995). How do thalamic axons find their way to the cortex? Trends Neurosci *18*, 389-397.

Molnár, Z., Luhmann, H.J., and Kanold, P.O. (2020). Transient cortical circuits match spontaneous and sensory-driven activity during development. Science *370*.

Molyneaux, B.J., Goff, L.A., Brettler, A.C., Chen, H.H., Hrvatin, S., Rinn, J.L., and Arlotta, P. (2015). DeCoN: genome-wide analysis of in vivo transcriptional dynamics during pyramidal neuron fate selection in neocortex. Neuron *85*, 275-288.

Muzumdar, M.D., Tasic, B., Miyamichi, K., Li, L., and Luo, L. (2007). A global double-fluorescent Cre reporter mouse. Genesis *45*, 593-605.

Nowakowski, T.J., Bhaduri, A., Pollen, A.A., Alvarado, B., Mostajo-Radji, M.A., Di Lullo, E., Haeussler, M., Sandoval-Espinosa, C., Liu, S.J., Velmeshev, D.*, et al.* (2017). Spatiotemporal gene expression trajectories reveal developmental hierarchies of the human cortex. Science *358*, 1318-1323.

Oeschger, F.M., Wang, W.Z., Lee, S., Garcia-Moreno, F., Goffinet, A.M., Arbones, M.L., Rakic, S., and Molnar, Z. (2012). Gene expression analysis of the embryonic subplate. Cereb Cortex *22*, 1343-1359.

Olave, I., Wang, W., Xue, Y., Kuo, A., and Crabtree, G.R. (2002). Identification of a polymorphic, neuron-specific chromatin remodeling complex. Genes Dev *16*, 2509-2517.

Ozaki, H.S., and Wahlsten, D. (1992). Prenatal formation of the normal mouse corpus callosum: a quantitative study with carbocyanine dyes. J Comp Neurol *323*, 81-90.

Ozaki, H.S., and Wahlsten, D. (1998). Timing and origin of the first cortical axons to project through the corpus callosum and the subsequent emergence of callosal projection cells in mouse. J Comp Neurol *400*, 197-206.

Pearlman, A.L., and Sheppard, A.M. (1996). Extracellular matrix in early cortical development. Prog Brain Res *108*, 117-134.

Pedregosa, F., Varoquaux, G., Gramfort, A., Michel, V., Thirion, B., Grisel, O., Blondel, M., Prettenhofer, P., Weiss, R., and Dubourg, V. (2011). Scikit-learn: Machine learning in Python. the Journal of machine Learning research *12*, 2825-2830.

Piñon, M.C., Jethwa, A., Jacobs, E., Campagnoni, A., and Molnár, Z. (2009). Dynamic integration of subplate neurons into the cortical barrel field circuitry during postnatal development in the Golli-tau-eGFP (GTE) mouse. J Physiol *587*, 1903-1915.

Price, D.J., Aslam, S., Tasker, L., and Gillies, K. (1997). Fates of the earliest generated cells in the developing murine neocortex. J Comp Neurol *377*, 414-422.

Rakic, P. (1974). Neurons in rhesus monkey visual cortex: systematic relation between time of origin and eventual disposition. Science *183*, 425-427.

Rakic, S., Davis, C., Molnar, Z., Nikolic, M., and Parnavelas, J.G. (2006). Role of p35/Cdk5 in preplate splitting in the developing cerebral cortex. Cereb Cortex *16 Suppl 1*, i35-45.

Ratie, L., Desmaris, E., Garcia-Moreno, F., Hoerder-Suabedissen, A., Kelman, A., Theil, T., Bellefroid, E.J., and Molnar, Z. (2019). Loss of Dmrt5 Affects the Formation of the Subplate and Early Corticogenesis. Cereb Cortex.

Robinson, M.D., McCarthy, D.J., and Smyth, G.K. (2010). edgeR: a Bioconductor package for differential expression analysis of digital gene expression data. Bioinformatics *26*, 139-140.

Ronan, J.L., Wu, W., and Crabtree, G.R. (2013). From neural development to cognition: unexpected roles for chromatin. Nat Rev Genet *14*, 347-359.

Routh, A., Head, S.R., Ordoukhanian, P., and Johnson, J.E. (2015). ClickSeq: Fragmentation-Free Next-Generation Sequencing via Click Ligation of Adaptors to Stochastically Terminated 3'-Azido cDNAs. J Mol Biol *427*, 2610-2616.

Sanders, S.J., He, X., Willsey, A.J., Ercan-Sencicek, A.G., Samocha, K.E., Cicek, A.E., Murtha, M.T., Bal, V.H., Bishop, S.L., Dong, S.*, et al.* (2015). Insights into Autism Spectrum Disorder Genomic Architecture and Biology from 71 Risk Loci. Neuron *87*, 1215-1233.

Serati, M., Delvecchio, G., Orsenigo, G., Mandolini, G.M., Lazzaretti, M., Scola, E., Triulzi, F., and Brambilla, P. (2019). The Role of the Subplate in Schizophrenia and Autism: A Systematic Review. Neuroscience *408*, 58-67.

Shatz, C.J., and Luskin, M.B. (1986). The relationship between the geniculocortical afferents and their cortical target cells during development of the cat's primary visual cortex. J Neurosci *6*, 3655-3668.

Sheppard, A.M., Hamilton, S.K., and Pearlman, A.L. (1991). Changes in the distribution of extracellular matrix components accompany early morphogenetic events of mammalian cortical development. J Neurosci *11*, 3928-3942.

Shi, L., Qalieh, A., Lam, M.M., Keil, J.M., and Kwan, K.Y. (2019). Robust elimination of genome-damaged cells safeguards against brain somatic aneuploidy following Knl1 deletion. Nat Commun *10*, 2588.

Shinmyo, Y., Asrafuzzaman Riyadh, M., Ahmed, G., Bin Naser, I., Hossain, M., Takebayashi, H., Kawasaki, H., Ohta, K., and Tanaka, H. (2015). Draxin from neocortical neurons controls the guidance of thalamocortical projections into the neocortex. Nat Commun *6*, 10232.

Smith, T., Heger, A., and Sudbery, I. (2017). UMI-tools: modeling sequencing errors in Unique Molecular Identifiers to improve quantification accuracy. Genome Res *27*, 491-499.

Sokpor, G., Xie, Y., Rosenbusch, J., and Tuoc, T. (2017). Chromatin Remodeling BAF (SWI/SNF) Complexes in Neural Development and Disorders. Front Mol Neurosci *10*, 243.

Son, E.Y., and Crabtree, G.R. (2014). The role of BAF (mSWI/SNF) complexes in mammalian neural development. Am J Med Genet C Semin Med Genet *166c*, 333-349.

Subach, O.M., Cranfill, P.J., Davidson, M.W., and Verkhusha, V.V. (2011). An enhanced monomeric blue fluorescent protein with the high chemical stability of the chromophore. PLoS One *6*, e28674.

Sunkin, S.M., Ng, L., Lau, C., Dolbeare, T., Gilbert, T.L., Thompson, C.L., Hawrylycz, M., and Dang, C. (2013). Allen Brain Atlas: an integrated spatio-temporal portal for exploring the central nervous system. Nucleic Acids Res *41*, D996-d1008.

Suzuki, K., Tsunekawa, Y., Hernandez-Benitez, R., Wu, J., Zhu, J., Kim, E.J., Hatanaka, F., Yamamoto, M., Araoka, T., Li, Z.*, et al.* (2016). In vivo genome editing via CRISPR/Cas9 mediated homology-independent targeted integration. Nature *540*, 144-149.

Tiong, S.Y.X., Oka, Y., Sasaki, T., Taniguchi, M., Doi, M., Akiyama, H., and Sato, M. (2019). Kcnab1 Is Expressed in Subplate Neurons With Unilateral Long-Range Inter-Areal Projections. Front Neuroanat *13*, 39.

Trizzino, M., Barbieri, E., Petracovici, A., Wu, S., Welsh, S.A., Owens, T.A., Licciulli, S., Zhang, R., and Gardini, A. (2018). The Tumor Suppressor ARID1A Controls Global Transcription via Pausing of RNA Polymerase II. Cell Rep *23*, 3933-3945.

Visel, A., Thaller, C., and Eichele, G. (2004). GenePaint.org: an atlas of gene expression patterns in the mouse embryo. Nucleic Acids Res *32*, D552-556.

Wagner, F., Yan, Y., and Yanai, I. (2018). K-nearest neighbor smoothing for high-throughput single-cell RNA-Seq data. bioRxiv, 217737.

Wang, W.Z., Hoerder-Suabedissen, A., Oeschger, F.M., Bayatti, N., Ip, B.K., Lindsay, S., Supramaniam, V., Srinivasan, L., Rutherford, M., Møllgård, K.*, et al.* (2010). Subplate in the developing cortex of mouse and human. J Anat *217*, 368-380.

Waskom, M., and seaborn development team, t. (2020). mwaskom/seaborn (Zenodo).

Wess, J.M., Isaiah, A., Watkins, P.V., and Kanold, P.O. (2017). Subplate neurons are the first cortical neurons to respond to sensory stimuli. Proc Natl Acad Sci U S A *114*, 12602-12607.

Yao, X., Wang, X., Hu, X., Liu, Z., Liu, J., Zhou, H., Shen, X., Wei, Y., Huang, Z., Ying, W.*, et al.* (2017). Homology-mediated end joining-based targeted integration using CRISPR/Cas9. Cell Res *27*, 801-814.

Yue, F., Cheng, Y., Breschi, A., Vierstra, J., Wu, W., Ryba, T., Sandstrom, R., Ma, Z., Davis, C., Pope, B.D., *et al.* (2014). A comparative encyclopedia of DNA elements in the mouse genome. Nature *515*, 355-364.

Yuzwa, S.A., Borrett, M.J., Innes, B.T., Voronova, A., Ketela, T., Kaplan, D.R., Bader, G.D., and Miller, F.D. (2017). Developmental Emergence of Adult Neural Stem Cells as Revealed by Single-Cell Transcriptional Profiling. Cell Rep *21*, 3970-3986.

Zhuo, L., Theis, M., Alvarez-Maya, I., Brenner, M., Willecke, K., and Messing, A. (2001). hGFAP-cre transgenic mice for manipulation of glial and neuronal function in vivo. Genesis *31*, 85-94.

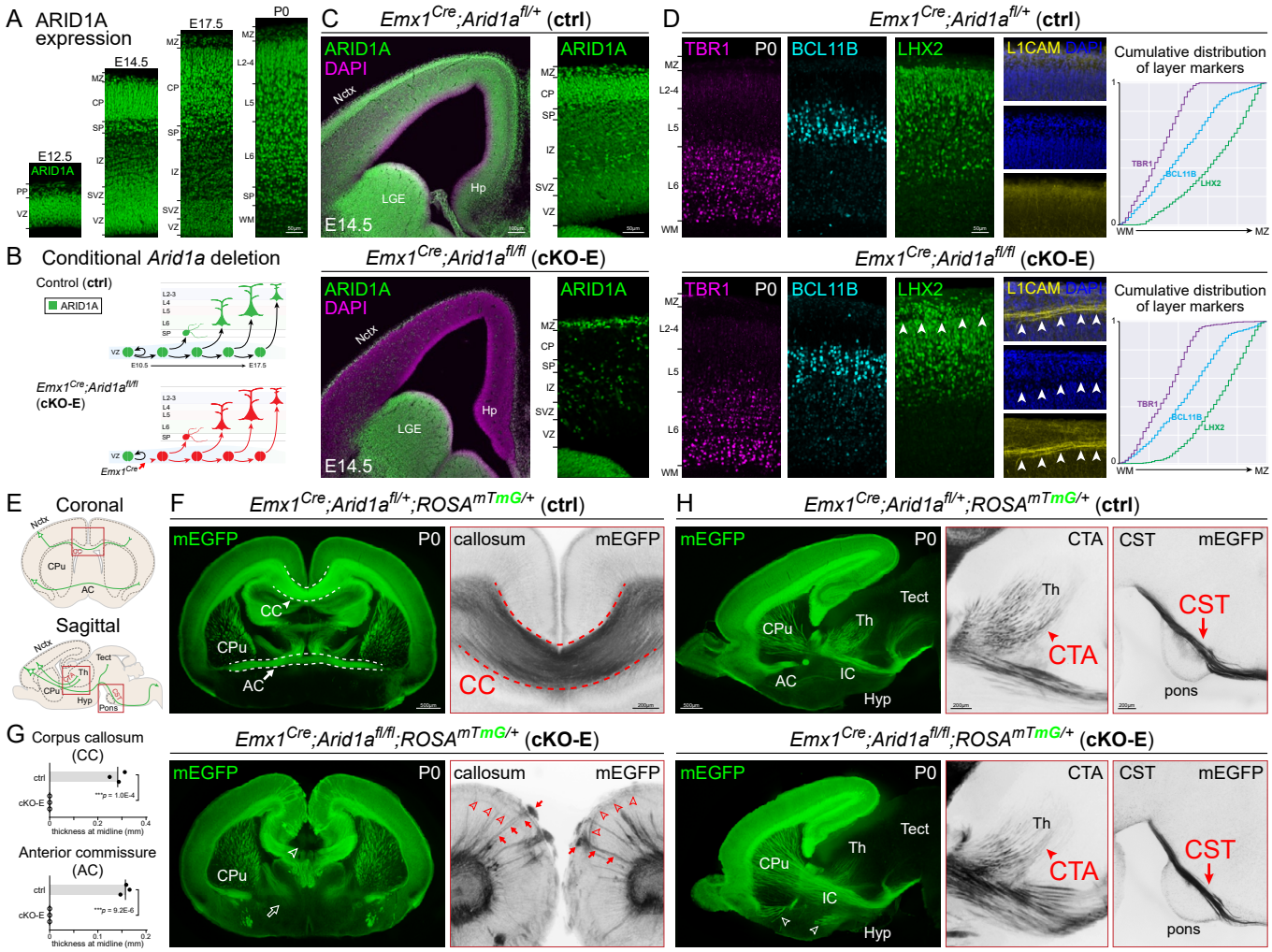

Figure 1 | Tract-dependent misrouting of cortical axons following conditional *Arid1a* deletion

A. ARID1A (green) immunostaining on coronal embryonic day (E)12.5, E14.5, E17.5, and postnatal day (P)0 brain sections revealed widespread ARID1A expression during cortical development. VZ, ventricular zone; SVZ, subventricular zone; PP, preplate; IZ, intermediate zone; SP, subplate; CP, cortical plate; MZ, marginal zone; Ln, layer n; WM, white matter

B. Schematic illustration of conditional *Arid1a* deletion using *Emx1*^{Cre}, which mediates recombination in cortical NPCs at E10.5, near the onset of neurogenesis.

C. ARID1A (green) and DAPI (magenta) staining of coronal E14.5 *Emx1*^{Cre}*;Arid1a*$^{fl/fl}$ (cKO-E) brain sections revealed loss of ARID1A from VZ and SVZ NPCs and CP neurons derived from *Emx1* lineage. ARID1A expression was unaffected in ventral forebrain. Nctx, neocortex; Hp, hippocampus; LGE, lateral ganglionic eminence

D. Layer marker immunostaining on coronal P0 brain sections. TBR1+ (L6, magenta), BCL11B+ (L5, cyan), and LHX2+ (L2-5, green) neurons were correctly ordered in cKO-E. Analysis of cumulative distribution of layer marker-expressing neurons through thickness of cortex from white matter (WM) to marginal zone (MZ) revealed no disruption in cortical lamination in cKO-E (n=3 animals). In all analyzed cKO-E brains (3/3 animals), but none of the littermate control (ctrl) brains (0/3 animals), a stereotyped gap (arrowheads) in the upper cortical layers was observed in LHX2 and DAPI (blue) staining. This gap contained misrouted L1CAM+ (yellow) axons.

E. Schematic illustration of cortical axon tracts on coronal and sagittal brain sections. CC, corpus callosum; AC, anterior commissure; CPu, caudate putamen; CTA, corticothalamic axons; CST, corticospinal tract; Tect, tectum; Hyp, hypothalamus

F. Coronal sections of P0 ctrl and cKO-E brains. Membrane EGFP (mEGFP, green) was expressed Cre-dependently from *ROSA*^{mTmG}, enabling anterograde tracing of cortical axons. Agenesis of corpus callosum (open arrowhead) was observed in cKO-E (n=3/3 animals). The anterior commissure also failed to form (open arrow). The cKO-E cortex was characterized by widespread axon misrouting (n=3/3 animals), including radially-directed axons extending to the pia (red arrows) and tangentially-directed axons travelling across the upper cortical layers (red arrowheads).

G. Quantification of corpus callosum and anterior commissure thickness at midline (data are mean, two-tailed unpaired *t* test, n=3 animals).

H. Sagittal sections of P0 ctrl and cKO-E brains. In cKO-E, corticofugal axons innervated internal capsule (IC) without defect. The trajectories of corticothalamic axons (CTA, red arrowheads), corticotectal axons, and corticospinal tract axons (CST, red arrows) were unaffected in cKO-E. Axons from anterior commissure (AC) were misrouted to hypothalamus (Hyp, open arrowheads).

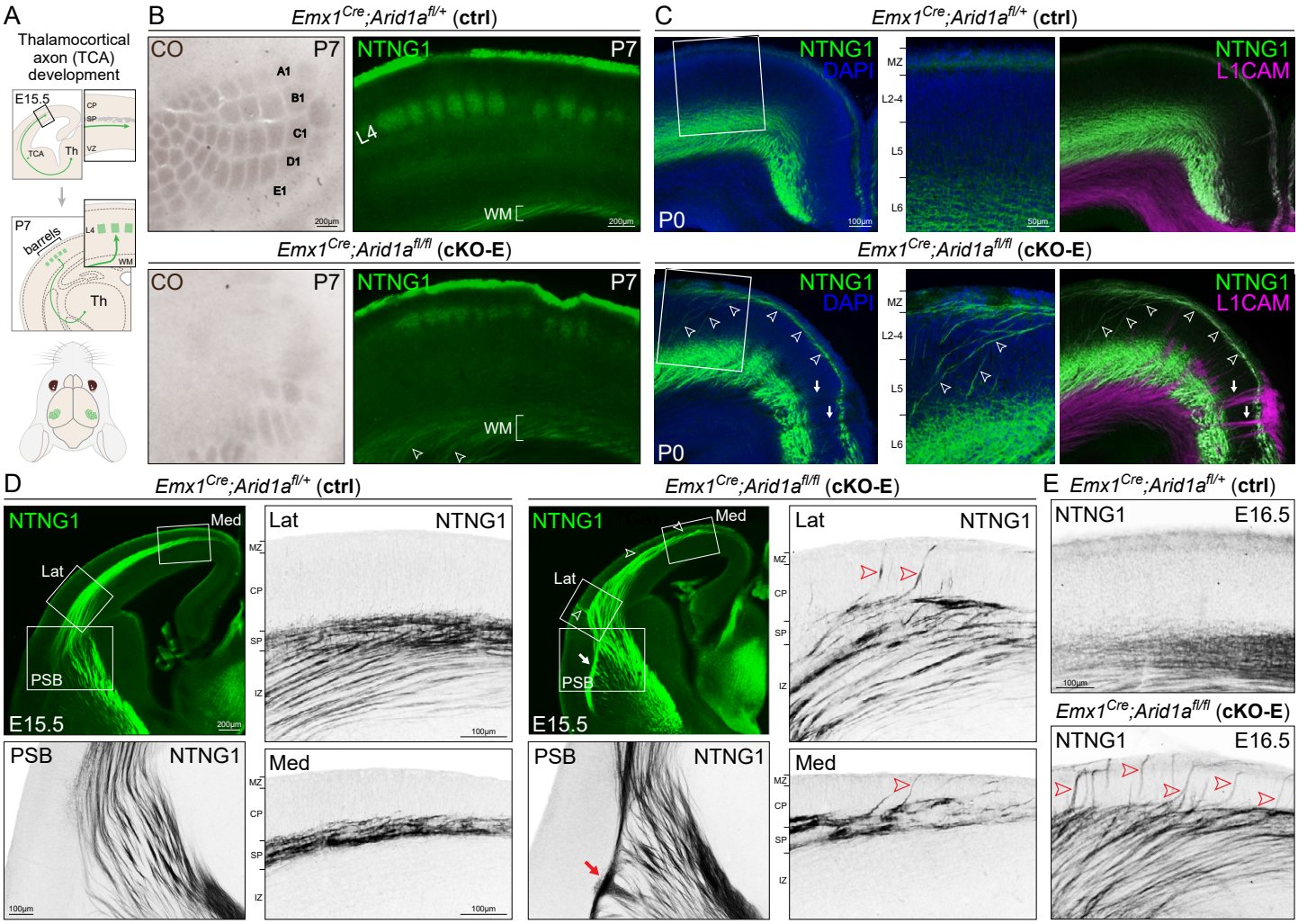

Figure 2 | Non-cell autonomous disruption of thalamocortical axon pathfinding following *Arid1a* deletion

A. Schematic illustration of thalamocortical axon (TCA) development. Th, thalamus

B. Whisker barrels in P7 ctrl and cKO-E primary somatosensory cortex were visualized by cytochrome oxidase staining (CO, brown) on flattened cortices and NTNG1 immunostaining (green) on coronal sections. In cKO-E, barrel formation was severely disrupted (n=5/5 animals). Many barrels were missing and the remaining barrels were distorted or disorganized. NTNG1+ thalamocortical axons were defasciculated in cortical white matter (open arrowheads) in cKO-E.

C. NTNG1 immunostaining (green) on coronal sections of P0 ctrl and cKO-E brains. In ctrl, NTNG1+ thalamocortical axons were present in white matter and L6, as well as marginal zone (MZ). In cKO-E, NTNG1+ thalamocortical axons were markedly misrouted, extending dorsally from white matter through the cortical layers (arrowheads). These aberrant axons then travelled tangentially across the upper layers and toward the midline. NTNG1+ thalamocortical axons did not contribute to the abnormal radially-directed axon bundles labeled by L1CAM (magenta, arrows) in cKO-E.

D. Analysis of thalamocortical axon development in E15.5 ctrl and cKO-E cortex. In ctrl, NTNG1+ thalamocortical axons extended across the pallial-subpallial boundary (PSB) and were paused within the subplate (SP) during the embryonic "waiting" period. In cKO-E, NTNG1+ thalamocortical axons did not cross the PSB along the normal trajectory (n=3/3 animals). They formed an aberrant bundle of axons parallel to the PSB (red arrow) and entered the cortex via an abnormal dorsal path. Notably, NTNG1+ thalamocortical axons prematurely invaded the cortical plate (CP) in both lateral (Lat) and medial (Med) cortex (red arrowheads) (n=3/3 animals). The trajectory of these axons was similar to that of the misrouted thalamocortical axons in the P0 cKO-E cortex (arrowheads in **C**).

D. Analysis of E16.5 ctrl and cKO-E cortex revealed an abundance of NTNG1+ thalamocortical axons prematurely invading the cortical plate (red arrowheads).

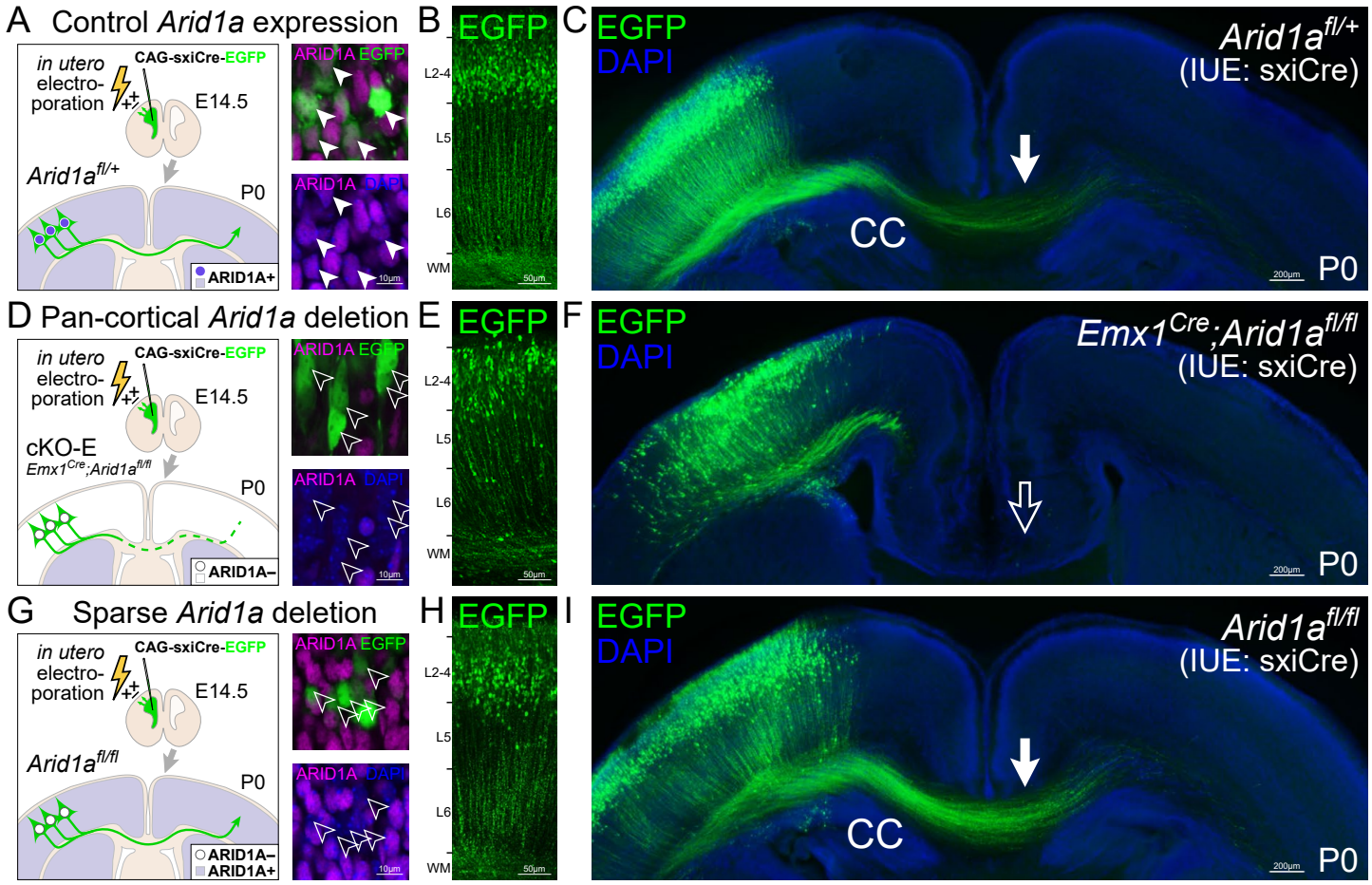

Figure 3 | Correct callosal axon targeting following sparse deletion of *Arid1a*

A self-excising Cre expression, EGFP reporter construct (CAG-sxiCre-EGFP) was transfected into dorsal cortical NPCs of *Arid1a*$^{fl/+}$ (control, **A**), *Emx1*^{Cre}*;Arid1a*$^{fl/fl}$ (cKO-E, **D**), and *Arid1a*$^{fl/fl}$ (without genetic Cre, **G**) using *in utero* electroporation at E14.5. At P0, ARID1A expression (magenta) was analyzed in EGFP+ transfected cells by immunostaining. ARID1A was present in transfected control EGFP+ cells (solid arrowheads, **A**), but was lost following pan-cortical genetic *Arid1a* deletion (cKO-E, open arrowheads, **D**) or sparse *Arid1a* deletion (*Arid1a*$^{fl/fl}$, open arrowheads, **G**). EGFP+ cells migrated correctly to the upper cortical layers in each condition (**B**, **E**, **H**). EGFP+ axons innervated the corpus callosum (CC) in control (solid arrow, **C**), but failed to do so following broad *Arid1a* deletion in cKO-E (open arrow, **F**). Remarkably, sparse deletion of *Arid1a* from *Arid1a*$^{fl/fl}$ EGFP+ cells did not disrupt their innervation of the corpus callosum (solid arrow, **I**). Loss of ARID1A expression from these cells (open arrowheads, **G**) following sparse *Arid1a* deletion did not cell autonomously cause a callosal axon misrouting defect.

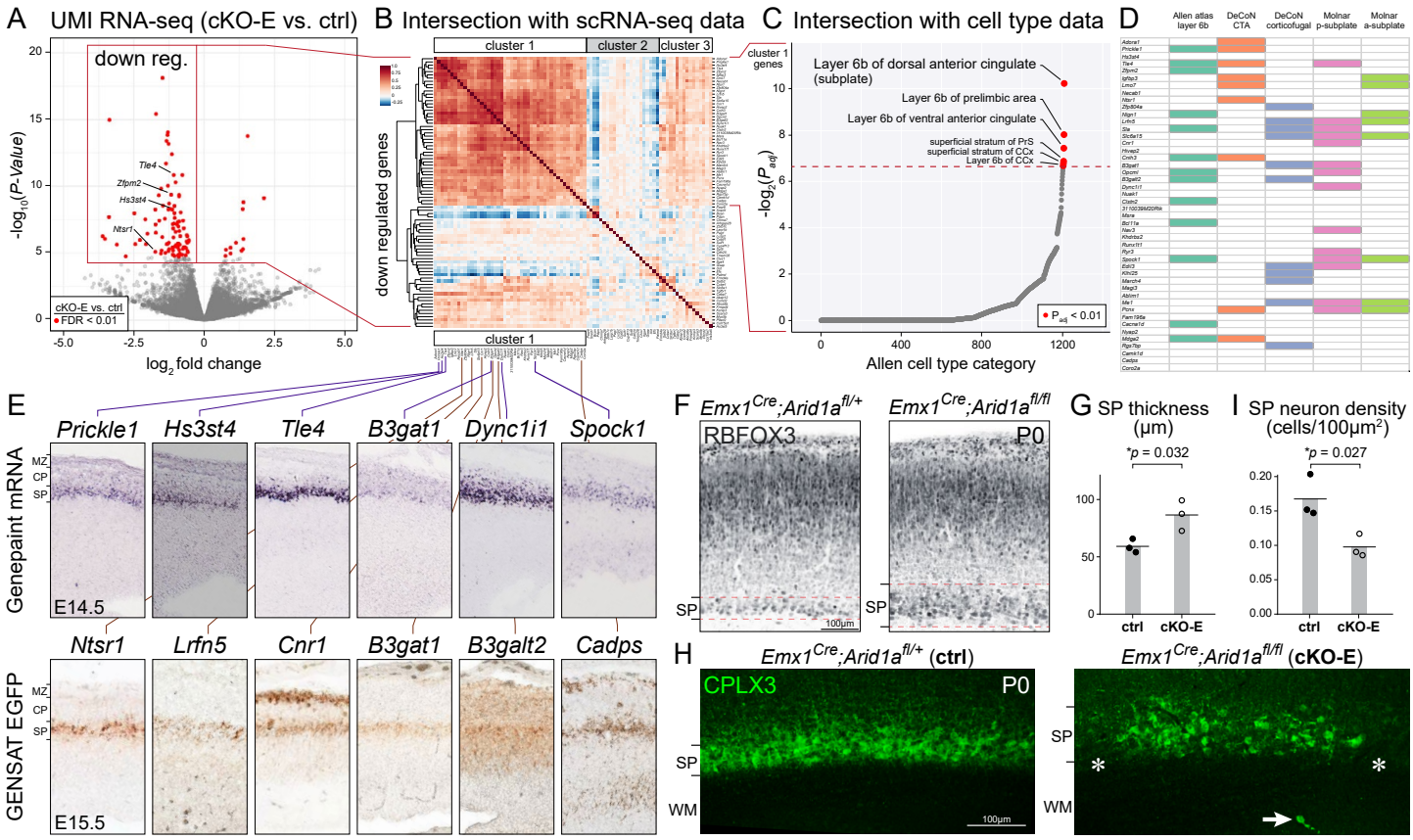

Figure 4 | Selective disruption of subplate neuron gene expression following *Arid1a* deletion

A. Volcano plot of unique molecular identifier (UMI) RNA-seq data comparing E15.5 cortex of cKO-E (n=6 animals) to ctrl littermates (n=6 animals). For each gene, P-value was calculated with likelihood ratio tests and false discovery rate (FDR) was calculated using the Benjamini-Hochberg procedure. Differentially expressed genes (FDR<0.01) are indicated by red dots. Of the 103 differentially expressed genes, 91 were downregulated and 12 were upregulated in cKO-E.
B. Intersectional analysis of significantly downregulated genes with single cell (sc)RNA-seq data from wildtype embryonic forebrain (Yuzwa et al., 2017). Unsupervised hierarchical clustering revealed a cluster of 46 downregulated genes (cluster 1) that are normally highly co-expressed at the level of single cells, suggesting that they may be expressed in one cell type.
C. Intersectional analysis of the 46 genes in cluster 1 with spatiotemporal gene expression dataset covering over 1200 brain subregions, including fetal brain (Sunkin et al., 2013). Cluster 1 showed a significant overrepresentation of genes selectively expressed in cortical layer 6b. Layer 6b is alternative nomenclature for subplate.
D. Intersectional analyses with orthogonal datasets (Molyneaux et al., 2015; Oeschger et al. 2012, Sunkin et al., 2013) confirmed subplate expression of genes in cluster 1.
E. Subplate expression of cluster 1 genes was further confirmed by E14.5 *in situ* hybridization data from the Genepaint database and E15.5 EGFP transgene expression data from the GENSAT consortium (Gong et al., 2003; Visel et al., 2004).
F. RBFOX3 immunostaining on coronal sections of P0 ctrl revealed a distinct and organized subplate band positioned just beneath the cortical layers. In cKO-E, the subplate band was thicker and less clearly defined.
G. Quantification of subplate (SP) thickness revealed significant subplate thickening in cKO-E (data are mean, two-tailed unpaired *t* test, n=3 animals).
H. CPLX3 immunostaining (green) on coronal sections of P0 ctrl and cKO-E brains. In ctrl, CPLX3+ subplate neurons were organized into a discrete, continuous band. In cKO-E, the band of CPLX3+ subplate neurons was more dispersed and characterized by gaps (asterisks). Some CPLX3+ cells aberrantly positioned in the white matter (WM, arrow).
I. Quantification revealed a significant decrease in CPLX3+ subplate neuron density in cKO-E (data are mean, two-tailed unpaired *t* test, n=3 animals).

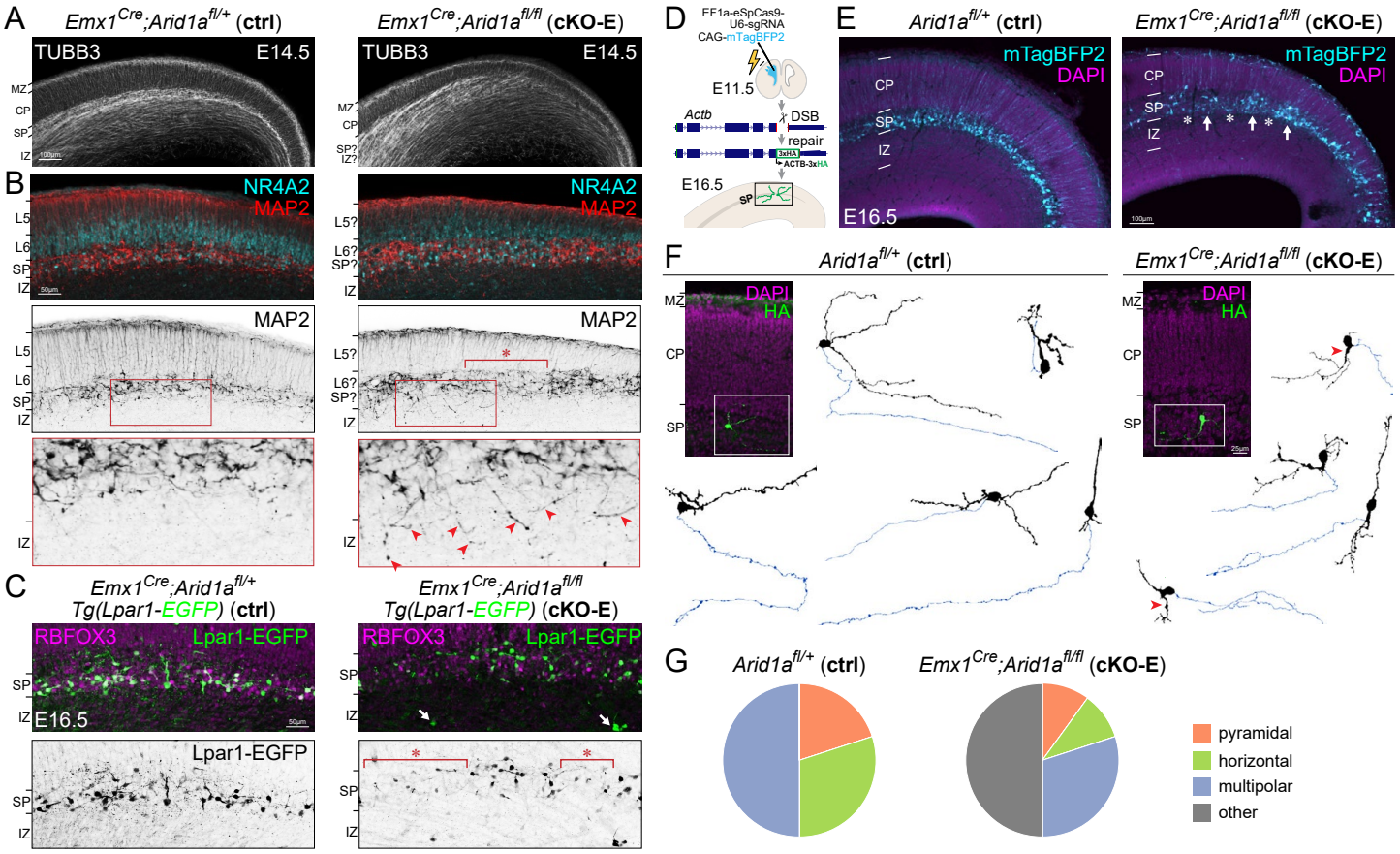

Figure 5 I Disrupted subplate organization and subplate neuron morphology following *Arid1a* deletion

A. TUBB3 (TUJ1) immunostaining on E14.5 ctrl and cKO-E sections. In ctrl, TUBB3+ processes were horizontally organized in intermediate zone (IZ) and subplate, and radially organized in cortical plate (CP). In cKO-E, TUBB3+ axons became defasciculated in intermediate zone, and invaded cortical plate diagonally.

B. MAP2 (red, black) and NR4A2 (cyan) immunostaining on E14.5 ctrl and cKO-E sections. In ctrl, MAP2+/NR4A2+ subplate neurons were organized within a clearly delineated layer below cortical plate. In cKO-E, subplate neurons were characterized by abnormal clustering and cell-sparse gaps (asterisk). In cKO-E, misoriented MAP2+ dendrites aberrantly projected ventrally into intermediate zone (red arrowheads, inset).

C. RBFOX3 (NEUN) immunostaining (magenta) on E16.5 ctrl and cKO-E brains carrying the *Lpar1-EGFP* transgene. In cKO-E, Lpar1-EGFP+ subplate neurons (green, black) were characterized by cell-sparse gaps (asterisks) and a few Lpar1-EGFP+ neurons were aberrantly positioned in the intermediate zone (arrows).

D. Schematic illustration of sparse subplate neuron labeling by *in utero* genome editing. A DNA break was induced by CRISPR-Cas9 within the coding region of *Actb* near the C-terminus. A reporter repair template was designed such that correct DNA repair would lead to expression of ACTB-3xHA. CRISPR-Cas9, reporter repair, and mTagBFP2 expression constructs were co-transfected into cortical NPCs at E11.5 by *in utero* electroporation (IUE). Electroporated brains were analyzed at E16.5.

E. In electroporated E16.5 brains, mTagBFP2 (cyan) was successfully targeted to subplate neurons. In cKO-E, labeled subplate neurons showed disorganization with abnormal cell clusters (arrows) and cell-sparse gaps (asterisks)

F. HA immunostaining (green) revealed the complete morphology of sparsely-labeled subplate neurons. Neurons were reconstructed based on confocal Z-stacks. Dendrites are indicated in black. Axons are indicated in blue. In cKO-E, some neurons were characterized by a dendrite ventrally directed into the intermediate zone (red arrowheads)

G. Quantification of subplate neuron morphological subclasses.

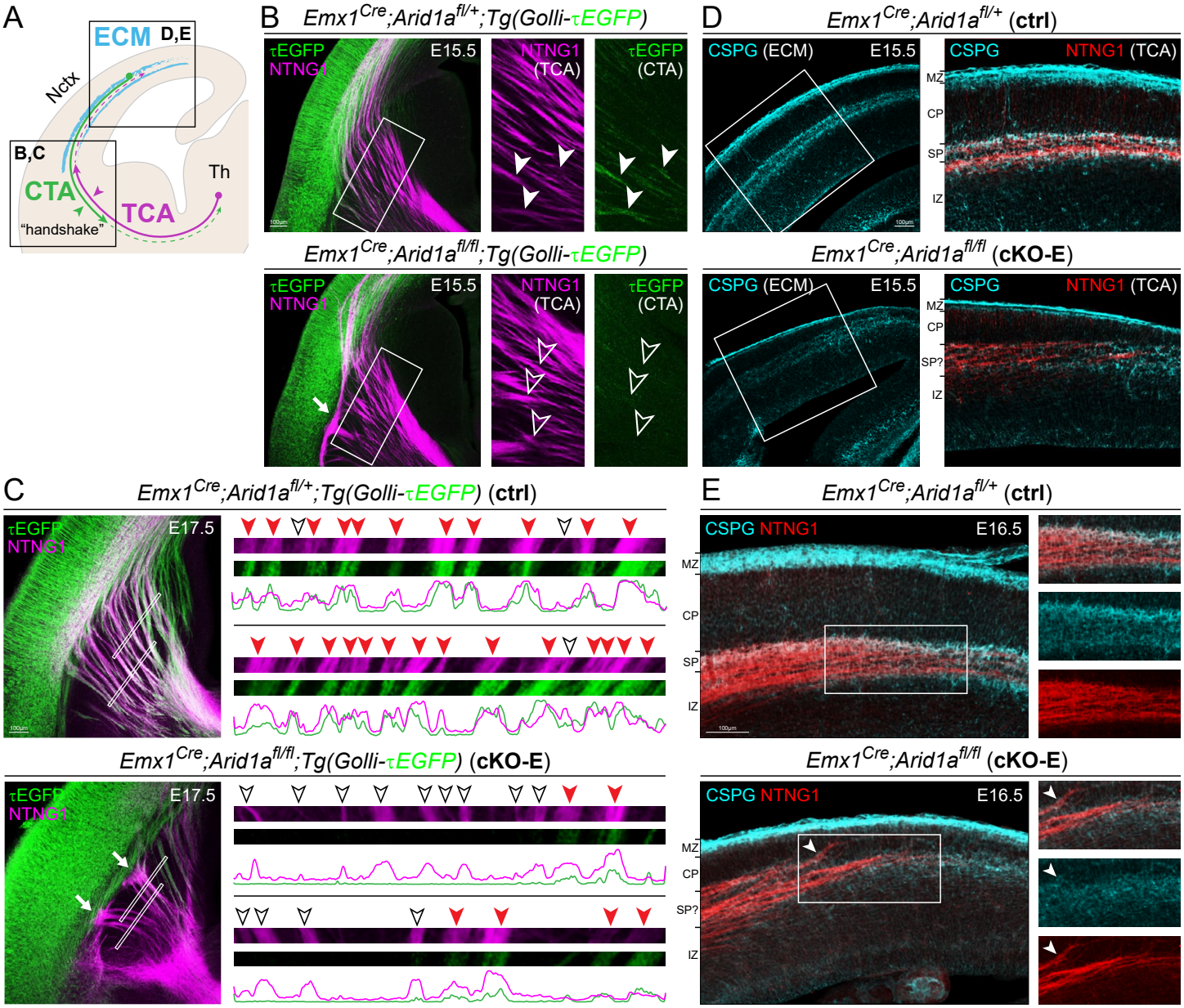

Figure 6 | Aberrant subplate neuron axon projection and extracellular matrix following *Arid1a* deletion

A. Schematic illustration of subplate neuron functions. CTA, corticothalamic axon; ECM, extracellular matrix

B, C. NTNG1 immunostaining (magenta) on E15.5 (**B**) and E17.5 (**C**) ctrl and cKO-E brains carrying the *Golli-τEGFP* transgene. In E15.5 ctrl, τEGFP+ (green) descending axons from subplate neurons closely cofasciculated (solid arrowheads) with ascending NTNG1+ thalamocortical axons (magenta). In E15.5 cKO-E, τEGFP+ axons largely have not crossed the pallial-subpallial boundary (PSB), and NTNG1+ axons did not cofasciculate with τEGFP+ axons (open arrowheads). NTNG1+ thalamocortical axons did not cross the PSB along the normal trajectory, forming an aberrant bundle parallel to the boundary (solid arrow) in cKO-E. In E17.5 ctrl, analysis of cofasciculation (insets) revealed frequent cofasciculation (red arrowheads) of τEGFP+ and NTNG1+ axons, which is consistent with the "handshake hypothesis". In E17.5 cKO-E, most NTNG1+ thalamocortical axons did not cofasciculate with τEGFP+ corticothalamic axons (open arrowheads) and were unable to cross the PSB (solid arrows).

D, E. CSPG (cyan) and NTNG1 (red) immunostaining on E15.5 (**D**) and E16.5 (**E**) ctrl and cKO-E brain sections. In ctrl, NTNG1+ thalamocortical axons tangentially traversed the embryonic cortex within a subplate/intermediate zone corridor neatly delineated by the extracellular matrix component CSPG. In cKO-E, CSPG expression was reduced and the CSPG corridor had collapsed. NTNG1+ thalamocortical axons were not confined within the subplate/intermediate zone, deviated from their normal trajectory, and prematurely invaded the cortical plate (arrowhead).

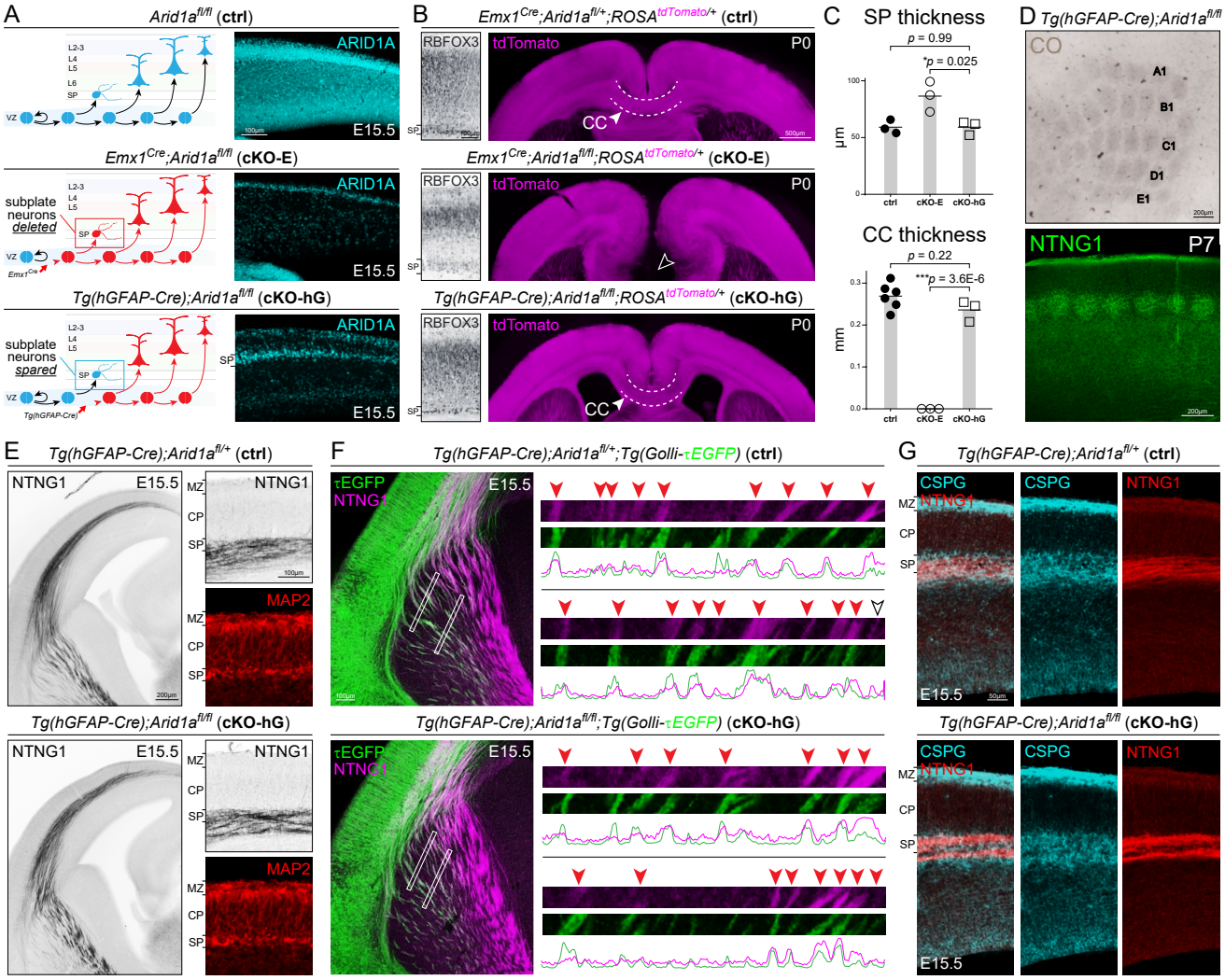

Figure 7 | Subplate-spared cortical plate deletion of *Arid1a*

A. Schematic illustration of subplate-spared cortical plate deletion of *Arid1a*. *Emx1*^{Cre} mediates Cre recombination in cortical NPCs starting at E10.5, prior to subplate neuronogenesis. ARID1A immunostaining (cyan) in E15.5 *Emx1*^{Cre}*;Arid1a*$^{fl/fl}$ (**cKO-E**) revealed loss of ARID1A from subplate and cortical plate neurons. Tg(*hGFAP-Cre*) mediates Cre recombination in cortical NPCs starting at E12.5, after the majority of subplate neurons have been generated. In E15.5 Tg(*hGFAP-Cre*);*Arid1a*$^{fl/fl}$ (**cKO-hG**), ARID1A was lost from cortical plate neurons, but present in subplate neurons.

B. Subplate and axon tract analyses on P0 ctrl, cKO-E, and cKO-hG brain sections. RBFOX3 immunostaining revealed in cKO-hG an organized, distinct subplate band positioned just beneath the cortical layers that was indistinguishable from ctrl. tdTomato (magenta) was expressed Cre-dependently from *ROSA*^{tdTomato}, enabling anterograde tracing of cortical axons. Agenesis of corpus callosum (open arrowhead) was observed in cKO-E. However, the corpus callosum (CC) was formed without defect in cKO-hG (solid arrowhead, n=3/3 animals).

C. Quantitative analyses revealed no significant changes in subplate thickness or corpus callosum thickness at midline in cKO-hG compared to ctrl (data are mean, ANOVA with Tukey's post hoc test, n≥3 animals).

D. Whisker barrels in cKO-hG primary somatosensory cortex were visualized by cytochrome oxidase staining (CO, brown) on flattened cortices and NTNG1 immunostaining (green) on coronal sections. Whisker barrels were formed without defect in cKO-hG (n=4/4 animals).

E. Analysis of thalamocortical axons and subplate neurons in E15.5 ctrl and cKO-hG cortex. In cKO-hG, NTNG1+ thalamocortical axons extended along a normal trajectory across the PSB, without forming an aberrant bundle parallel to the boundary. Upon reaching the cortex, NTNG1+ axons were correctly paused within subplate and did not prematurely invade cortical plate in cKO-hG. MAP2 immunostaining (red) revealed in cKO-hG subplate neurons that were organized within a continuous and clearly delineated layer below cortical plate.

F. NTNG1 immunostaining (magenta) on E15.5 ctrl and cKO-hG brains carrying the *Golli-τEGFP* transgene. In cKO-hG, τEGFP+ (green) descending axons from subplate neurons closely cofasciculated (red arrowheads) with ascending NTNG1+ thalamocortical axons (magenta).

G. CSPG (cyan) and NTNG1 (red) immunostaining on E15.5 ctrl and cKO-hG brain sections. In cKO-hG, NTNG1+ thalamocortical axons travelled within a subplate/intermediate zone corridor neatly delineated by the extracellular matrix component CSPG in a manner indistinguishable from ctrl.

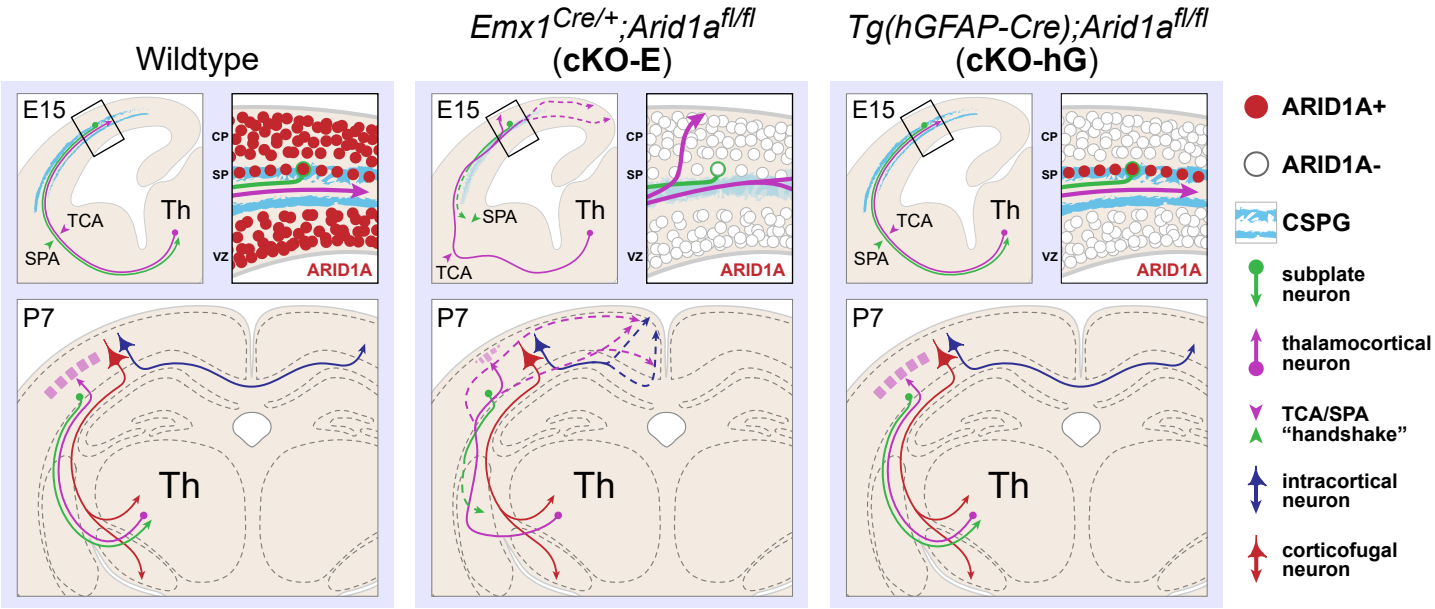

Figure 8 | Schematic summary of findings